Non-local topological valley Hall effect in bilayer graphene

Contents

Introduction

Suppose we start with a infinitely long strip of width W made of a standard conducting material. If we apply a voltage V at two opposite points of the strip a current will flow from one electrode to the other. The current will be the strongest along the segment that unites the electrodes, and will be exponentially weaker the further away it is. This off-axis current is called *Nonlocal Current* and it also generates a voltage along the edges of the strip called *Nonlocal Voltage*.
Experiments in high quality gapped graphene have highlighted the existence of a larger than expected nonlocal dc voltages.

The objective of this thesis is to first explain why this anomalous nonlocal current exists in gapped graphene, and develop a model that can be used to predict and analyze this kind of phenomenon.
The thesis is structured as follows:

The first chapter is devoted to explaining how some of the machinery we'll use work. This includes some of the main concepts of topology in solid state physics, like the Hall effect, Berry phase, Berry curvature. We then use the concept of Berry curvature to generalize the Hall effect and obtain the Kubo formula and the TKNN formula. We also give a quick overview of the electronic properties of graphene and derived like gapped graphene and bilayer graphene where we focus on what happens close to the Dirac points and we introduce the concept of *Valley*.

The second chapter is devoted to see how all this tools come together in fact the nonlocal current arises from the Berry curvature hot spots near the Dirac points in gapped graphene which give rise to a particular kind of anomalous Hall effect called *Valley Hall Effect*. This creates a transverse *Valley Current* that is responsible for the high nonlocal voltage measured in the experiments

In the third and last chapter we create a model that explains in full detail how the voltage and currents behave inside of a graphene strip and develop an approximation that can be used to evaluate the properties of these kind of system and apply it to data from real-world experiments.

Chapter 1

Introduction to relevant topics

1.1 Elementary introduction to topology in condensed matter physics

To start off we are goin to talk about a very specific case of a quantum particle in a ring around a infinitely long solenoid.

The hamiltonian of a particle with charge $-e$ moving through a magnetic field $\mathbf{B} = \nabla \times \mathbf{A}$ is

$$H = \frac{1}{2m}(\mathbf{p} + e\mathbf{A})^2 \tag{1.1}$$

Since

$$\mathbf{p} = p_\theta \hat{\theta} = -\frac{i\hbar\hat{\theta}}{R}\frac{\partial}{\partial\theta}$$

$$\oint \mathbf{A} \cdot d\mathbf{r} = \int \mathbf{B} \cdot d\mathbf{s} = \Phi$$

it means that

$$\mathbf{A} = \frac{\Phi}{2\pi R}\hat{\theta} \tag{1.2}$$

Putting it back into the hamiltonian

$$H = \frac{1}{2m}\left(-\frac{i\hbar}{R}\frac{\partial}{\partial\theta} + \frac{e\Phi}{2\pi R}\right)^2 \tag{1.3}$$

The eigenstates of this hamiltonian are

$$\psi_n(\theta) = \frac{e^{in\theta}}{\sqrt{2\pi R}}; \quad n \in \mathbb{Z}$$

Interestingly the Energies of the eigenstates are influenced by the vector potential

$$E_n = \frac{1}{2mR^2}\left(\hbar n + \frac{e\Phi}{2\pi}\right)^2 = \tilde{E}\left(n + \frac{\Phi}{\Phi_0}\right)^2 \tag{1.4}$$
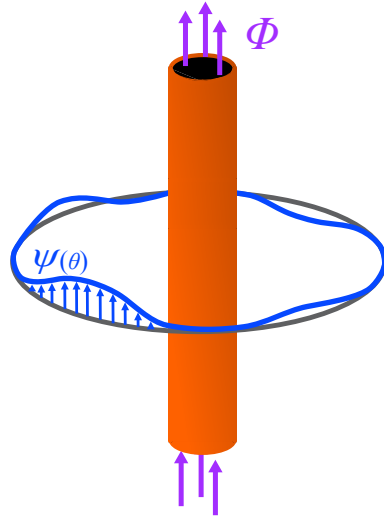
where

$$\tilde{E} = \frac{\hbar^2}{2mR^2} \quad \text{and} \quad \Phi_0 = \frac{2\pi\hbar}{e}$$

Suppose now that we start with the turned soleind off, and place the particle in the $n = 0$ ground state. If we increase the flux then, by the time we have reached $\Phi = \Phi_0$, the $n = 0$ state has transformed into the state that we previously labelled $n = 1$. Similarly, each state n is shifted to the next state, $n + 1$ [1].
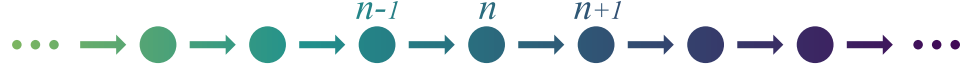
This is an example of a phenomenon is called spectral flow: under a change of parameter the spectrum of the Hamiltonian changes, or "flows". As we change increase the flux by one unit Φ_0 the spectrum returns to itself, but individual states have morphed into each other. [1]
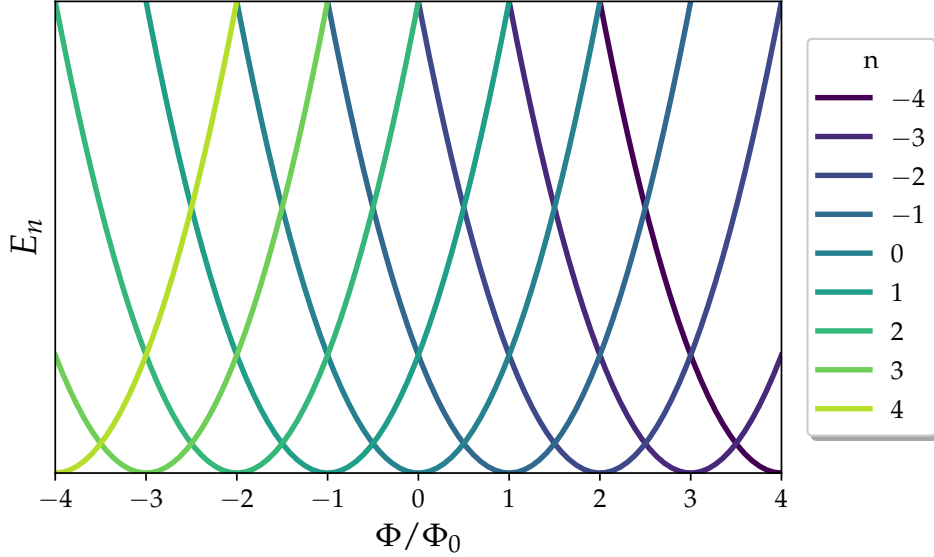
Figure 1.1: Here plotted the energies E_n (eq. 1.4), notice how the states *"flow"* as we change Φ

Parallelism with Bloch's Theorem

The keen eyed among you might have noticed that figure 1.1 is suspicially similar to a crystal band structure in the limit on which the periodic potential $V \to 0$ with periodicity 2π, let's see if this analogy holds *the test of math*.

---

[1]It is tempting to invoke the adiabatic theorem here but, because of level crossing at $\Phi = \Phi_0/2$ it is not valid

Let's start by taking the single-particle free propagating Hamiltonian

$$H = \frac{1}{2m}p_\theta^2$$

The eigenstates this time have to respect the condition that $u_{n,q}(\theta) = e^{i2\pi q}u_{n,q}(\theta + 2\pi)$.[2] This also means that if we substitute $q \to q + 1$ the spectrum doesn't change.

We now make the following unitary transformation to obtain a q-depentant Hamiltonian.

$$H(q) = e^{-iq\theta}He^{iq\theta} = \frac{1}{2m}\left(p_\theta + \frac{\hbar q}{R}\right)^2$$

We can easly map this hamiltonian to the one in equation 1.3 just by difining Φ such that $\hbar q = \frac{e\Phi}{2\pi}$.

$$H(\Phi) = \frac{1}{2m}\left(p_\theta + \frac{e\Phi}{2\pi R}\right)^2 \tag{1.5}$$

Since before we said that the system doesn't change if we substitute $q \to q+1$, it means that now the system remains unchanged if we send $\Phi \to \Phi + \Phi_0$. This is exactly the result obtained in the previous page.

And the tranformed eigenstates $\psi_{n,q} = e^{-iq\theta}u_{n,q}$ is just the cell-periodic part of the Bloch function. It satified the stricter periodic boundary condition

$$\psi_{n,q}(\theta) = \psi_{n,q}(\theta + 2\pi) \tag{1.6}$$

As you can see equations 1.5 and 1.6 create a system that is mathematically equivalent to the particle moving in a ring around a flux tube [2].

Conditions to have spectral flow

Up until now we looked spectral flow the case where the particle is freely propagating, let's see what happens when we add a periodic potential $V(\theta) = V(\theta + 2\pi)$

$$H = \frac{1}{2m}p_\theta^2 + V(\theta)$$

Now the spectrum is still periodic, however the energy bands don't necessarly cross, this means that when abiabatically changing q, (or equivalently Φ) the states won't flow, instead they will return to their original state Conversely if there are n degeneracies, on every cycle more the i-th stathe will flow to the $i + n$-th state

---

[2]This come from the block's theorem that states that the eigenstates of the hamiltonian of a periodic potential with periodicity a mush obey that $u_{n,q}(x) = e^{iaq}u_{n,q}(x + a)$. In our case the periodicity $a = 2\pi$ and the variable of the function is θ instead of x
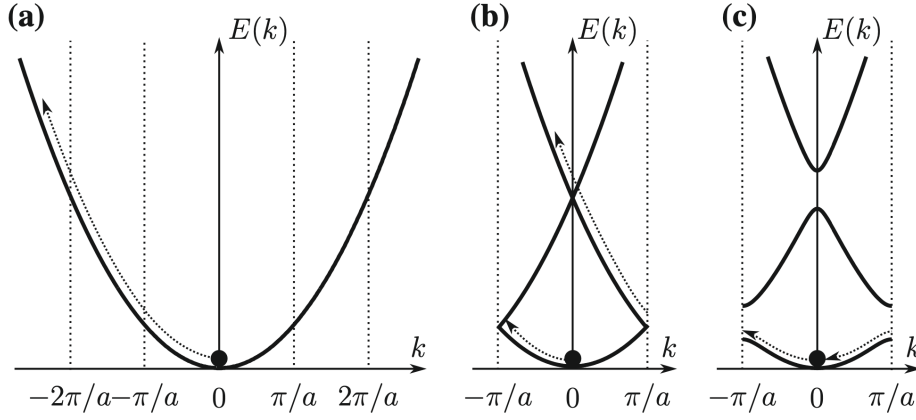
Figure 1.2: Pictorial representation of what happens when changing q

Spectral flow in a more general context

The spectral flow is applicable in much more complex geometries than the one we have seen so far.

Suppose that now the particle can moove in a 3D potential $V(\mathbf{r})$, the Hamiltonian is

$$H(\mathbf{A}) = \frac{1}{2m}(\mathbf{p} + e\mathbf{A})^2 + V(\mathbf{r})$$

Since the solenoid is still the same, the formula for $\mathbf{A}$ remains unchanged (eq. 1.2)

$$H(\Phi) = \frac{1}{2m}\left(\mathbf{p} + \frac{e\Phi}{2\pi R}\hat{\theta}\right)^2 + V(\mathbf{r})$$

and since it's expressed in cylindrical coordinates it's better to express also $\mathbf{p}$ in cylindrical coordinates.

$$\mathbf{p} = -i\hbar\nabla = -i\hbar\left(\hat{\mathbf{r}}\frac{\partial}{\partial r} + \frac{\hat{\theta}}{r}\frac{\partial}{\partial\theta} + \hat{\mathbf{z}}\frac{\partial}{\partial z}\right) \equiv \hat{\mathbf{r}}p_r + \hat{\theta}p_\theta + \hat{\mathbf{z}}p_z$$

Of course if we send $\theta \to \theta + 2\pi$ the system should be unchanged.

$$\psi(r, \theta, z) = \psi(r, \theta + 2\pi, z)$$

Following the inverse reasoning done in the previous subsection we make the following unitary transformation.

$$H = e^{i\theta\Phi/\Phi_0}H(\Phi)e^{-i\theta\Phi/\Phi_0} = \frac{\mathbf{p}^2}{2m} + V(\mathbf{r})$$

This means that the eigenvalue probelm is now written like so

$$He^{i\theta\Phi/\Phi_0}\psi(r,\theta,z) = E(\Phi)e^{i\theta\Phi/\Phi_0}\psi(r,\theta,z)$$

7

If we send $\Phi \rightarrow \Phi + \Phi_0$ we get an equivalent equation

$$He^{i\theta\Phi/\Phi_0}\psi(r,\theta,z) = E(\Phi + \Phi_0)e^{i\theta\Phi/\Phi_0}\psi(r,\theta,z)$$

this means that the energy spectrum is unchanged if we send $\Phi \rightarrow \Phi + \Phi_0$. This is true regardless of the shape or geometry of $V(\mathbf{r})$.
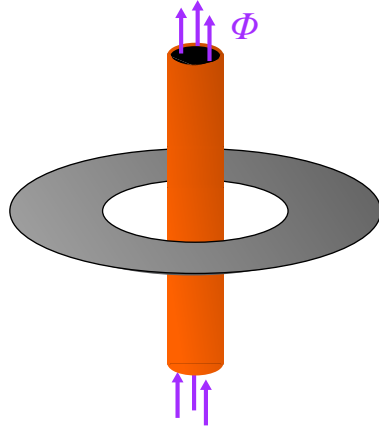
The quantum Hall effect

We'll now see the effects of the spectral flow on physical properties of materials. Suppose we have a system like the one of the figure on the side. Now we slowly increase Φ from 0 to Φ_0 in a total time T. This introduces a electromagnetice force arround the ring $\mathcal{E} = -\partial_t \Phi = -\Phi_0/T$.

Let's suppose that the disc has the property that due to spectral flow n electrons are transferred form the inner cirlce to the outer cicle in this time T. This would result in a radial current $I_r = -ne/T$. This means that the resistance is

$$R_{xy} = \frac{\mathcal{E}}{I_r} = \frac{2\pi\hbar}{e^2}\frac{1}{n} \qquad (1.7)$$

However, to be able to calculate n we need to calculate how is the spectrum of the system as we change Φ. This means that n depends on the system, but equation 1.7 is independent of the system. [3]

1.2 Berry phase

Berry phase is the simplest demonstration of how geometry and topology can emerge from quantum mechanics and at heart of the quantum Hall effect.
Let us consider a physical system described by a Hamiltonian that depends on a set of parameters $\boldsymbol{\lambda} = (\lambda_1, \lambda_2, \dots)$. These parameters do not represent the degrees of freedom of the system like position and momentum, rather they describe things such as the mass of a particle, the strength of a potential and so on.
For each $H(\boldsymbol{\lambda})$ there exists a set of eigenstates such that

$$H(\boldsymbol{\lambda})\,|n, \boldsymbol{\lambda}\rangle = E_n(\boldsymbol{\lambda})\,|n, \boldsymbol{\lambda}\rangle \qquad (1.8)$$

---

[3]There is the caveaut here that the system has to be in a defined quantum state, so in real world system it means that $T \approx 0$

However the equation above does not completely determine the basis function $|n, \boldsymbol{\lambda}\rangle$; We can change arbitrarily the phase $\gamma_n(\boldsymbol{\lambda})$ of any eigenstate which is called *Berry phase*

$$|n, \boldsymbol{\lambda}\rangle \rightarrow \underbrace{e^{i\gamma_n(\boldsymbol{\lambda})}}_{\text{Berry phase}} |n, \boldsymbol{\lambda}\rangle \qquad (1.9)$$

Suppose we start off with a Hamiltonian and then we slowly change the parameters for a time T until it reaches a different Hamiltonian, this means that $\boldsymbol{\lambda} = \boldsymbol{\lambda}(t)$. For the adiabatic theorem we can say that if we start on an energy eigenstate, and the system changes slowly enough, [4] and has no degeneracies, then the system will cling on that energy eigenstate.

This means that the equation of motion of a particle that for time $t = 0$ is equal to $|\psi_n(t=0)\rangle = |n, \boldsymbol{\lambda}(0)\rangle$ is

$$|\psi_n(t)\rangle = \underbrace{e^{i\gamma_n(\boldsymbol{\lambda}(t))}}_{\text{Berry phase}} \cdot \underbrace{e^{-\frac{i}{\hbar}\int_0^t E_n(\boldsymbol{\lambda}(t'))dt'}}_{\text{dynamical phase}} |n, \boldsymbol{\lambda}(t)\rangle \qquad (1.10)$$

Where the first exponent comes from eq. 1.9. We now insert the equation above into the time-dependent Shrodinger equation

$$i\hbar\partial_t|\psi_n(t)\rangle = H(\boldsymbol{\lambda}(t))|\psi_n(t)\rangle \qquad (1.11)$$

By plugging equation 1.10 into the *right* term term of equation 1.11 we get we get that

$$H(\boldsymbol{\lambda}(t))|\psi_n(t)\rangle = E_n(t)|\psi_n(t)\rangle \qquad (1.12)$$

Andy By plugging equation 1.10 into the *left* term term of equation 1.11 we get we get that

$$i\hbar\partial_t|\psi_n(t)\rangle = -\hbar\dot{\gamma}_n(t)|\psi_n(t)\rangle + E_n(t)|\psi_n(t)\rangle + e^{i\phi_n(t)}\partial_t|n,t\rangle \qquad (1.13)$$

where we have defined $e^{i\phi_n(t)} \equiv e^{i\gamma_n(\boldsymbol{\lambda}(t))}e^{-\frac{i}{\hbar}\int_0^t E_n(\boldsymbol{\lambda}(t'))dt'}$

By equating the right terms in equations 1.12 and 1.13 we get that

$$i\hbar e^{i\phi_n t(t)}\partial_t|n,t\rangle = \hbar\dot{\gamma}_n(t)|\psi_n(t)\rangle = \hbar\dot{\gamma}_n(t)e^{i\phi_n(t)}|n,t\rangle \qquad (1.14)$$

now we multiply the term on the left and on the right of equation 1.14 by $\hbar^{-1}e^{-i\phi_n(t)}\langle n,t|$

$$\dot{\gamma}_n(t) = i\langle n,t|\partial_t|n,t\rangle \qquad (1.15)$$

---

[4] How slow you have to be in changing the parameters depends on the energy gap from the state you're in to the nearest other state. The smaller the gap, the slower you have to change the parameters. A way of showing this without doing long calculations is the following:
We know from the Heisenberg uncertainty principle that $T\Delta E \geq \hbar/2$. We want the uncertainty in the Energy to be way smaller than the energy gap $E_g \gg \Delta E$, so $E_g \gg \frac{\hbar}{2T}$, therefore if we make T big enough it can be achieved

We can re-express it in terms of $\boldsymbol{\lambda}$

$$\dot{\gamma}_n(t) = \dot{\boldsymbol{\lambda}} \cdot \underbrace{i \langle n, t | \partial_{\boldsymbol{\lambda}} | n, t \rangle}_{\equiv \mathbf{A}_n(\boldsymbol{\lambda})} \tag{1.16}$$

Where $\mathbf{A}_n(\boldsymbol{\lambda})$ called the **Berry connection** This means that we can calculate the total change in $\gamma_n(t)$ can be obtained by doing a line integral in the space of parameters $\boldsymbol{\lambda}$ over the path $\mathcal{P}$ of values that $\boldsymbol{\lambda}$ assumes during the time evolution

$$\gamma_n = \int_{\mathcal{P}} \mathbf{A}_n(\boldsymbol{\lambda}) \cdot d\boldsymbol{\lambda} \tag{1.17}$$

$$|n, \boldsymbol{\lambda}\rangle \rightarrow e^{if_n(\boldsymbol{\lambda})} |n, \boldsymbol{\lambda}\rangle \tag{1.18}$$

Keep in mind however that the eigenstates are defined up to a phase, meaning that we can re-define the base vectors like so (equation 1.18). If we apply this substitution into the formula of $\mathbf{A}_n$ we have that

$$\mathbf{A}_n(\boldsymbol{\lambda}) = i \langle n, t | \partial_{\boldsymbol{\lambda}} | n, t \rangle \rightarrow i \langle n, t | \partial_{\boldsymbol{\lambda}} | n, t \rangle - \partial_{\boldsymbol{\lambda}} f_n(\boldsymbol{\lambda})$$

$$\mathbf{A}_n \rightarrow \mathbf{A}_n - \partial_{\boldsymbol{\lambda}} f_n \tag{1.19}$$

So the system is invariant under the gauge transformation in equation 1.19. If we do this transformation to equation 1.17 we have that

$$\gamma_n = \int_{\mathcal{P}} \mathbf{A}_n(\boldsymbol{\lambda}) \cdot d\boldsymbol{\lambda} - \int_{\mathcal{P}} \partial_{\boldsymbol{\lambda}} f_n(\boldsymbol{\lambda}) \cdot d\boldsymbol{\lambda} = \int_{\mathcal{P}} \mathbf{A}_n(\boldsymbol{\lambda}) \cdot d\boldsymbol{\lambda} + f(\boldsymbol{\lambda}(0)) - f(\boldsymbol{\lambda}(T))$$

This means that if the path $\mathcal{P}$ is open we can always choose a function f_n such that $f(\boldsymbol{\lambda}(0)) - f(\boldsymbol{\lambda}(T)) = \int_{\mathcal{P}} \mathbf{A}_n(\boldsymbol{\lambda}) \cdot d\boldsymbol{\lambda}$, thus we can conclude that one can always choose a suitable $f(\boldsymbol{\lambda})$ such that γ_n accumulated along the path $\mathcal{P}$ is calceled out leaving equation 1.10 with only the dynamical phase. However if the path is closed $\boldsymbol{\lambda}(0) = \boldsymbol{\lambda}(T)$, in order to make the phase change in equation 1.18 single value we must have that

$$e^{f(\boldsymbol{\lambda}(0)) - f(\boldsymbol{\lambda}(T))} = 1$$

so

$$f(\boldsymbol{\lambda}(0)) - f(\boldsymbol{\lambda}(T)) = 2n\pi \quad n \in \mathbb{R}$$

This leads us to the important result that

$$\gamma_n = \oint_{\mathcal{P}} \mathbf{A}_n(\boldsymbol{\lambda}) \cdot d\boldsymbol{\lambda} + 2n\pi \tag{1.20}$$

This time, if the line integral is not a multiple of 2π (and there is no reason why it should) there is no way of choosing a suitable f_n to cancel it out and the Berry phase in equation 1.10 is there to stay

1.3 Berry curvature

You might have noticed that equation 1.19 is analogous to what happens in Electromagnetism with the vector potential. This means that we can try using the same mathematics and see where it leads us. However, in classic and relativistic electromagnetism $\dim(\boldsymbol{A}_\mu)$ is equal to respectively 3 and 4, in the case of the Berry curvature it can have any integer value.

In EM from the gauge-dependent $\boldsymbol{A}$ are defined the gauge-indipendent field as follows:

1. in 3D the magnetic field is defined as follows $B_i = \epsilon_{ijk}\partial_j A_k$

2. in $(3+1)$D the Field tensor is defined as $F_{\mu\nu} = \partial_\mu A_\nu - \partial_\nu A_\mu$

In both cases the resulting field is asymmetric under the exchange of the indices of the derivative and the indices of the vector potential. This requirement is what makes the resulting field gauge independent.

With the same logic we can define a gauge field tensor derived from the Berry connection:

$$\boxed{\Omega^n_{\mu\nu} = \partial_\mu A^n_\nu(\boldsymbol{\lambda}) - \partial_\nu A^n_\mu(\boldsymbol{\lambda})} \tag{1.21}$$

This new field tensor is defined as **Berry curvature**, and it is gauge indipendent just like $\boldsymbol{B}$ and $F_{\mu\nu}$![5]

From now on it can be useful to introduce the external product operator $\wedge$ that act as follows: Given two vectors $\boldsymbol{v}$ and $\boldsymbol{w}$ we have that

$$\boldsymbol{v} \wedge \boldsymbol{w} \equiv v_\mu w_\nu - v_\nu w_\mu \tag{1.22}$$

With this definition we can write

$$\boldsymbol{\Omega}^n(\boldsymbol{\lambda}) = \nabla \wedge \boldsymbol{A}^n(\boldsymbol{\lambda}) \tag{1.23}$$

Other formulas for $\Omega_{\mu\nu}$

With a few mathematical steps it is possible to re cast the Berry curvature into a different form that might be useful later

$$\partial_\mu A^n_\mu = i\partial_\mu \langle n, \boldsymbol{\lambda}| \partial_\nu n, \boldsymbol{\lambda}\rangle = i\langle \partial_\mu n, \boldsymbol{\lambda}| \partial_\nu n, \boldsymbol{\lambda}\rangle + i\langle n, \boldsymbol{\lambda}| \partial_\mu\partial_\nu n, \boldsymbol{\lambda}\rangle$$

$$\boxed{\Omega^n_{\mu\nu} = i\langle \partial_\mu n| \partial_\nu n\rangle - i\langle \partial_\nu n| \partial_\mu n\rangle} \tag{1.24}$$

or, equivalently

$$\boldsymbol{\Omega}^n = i\langle \nabla n| \wedge |\nabla n\rangle \tag{1.25}$$

---

[5]The notation has changed a bit, now $A^n_\mu \equiv (\mathbf{A}_n)_\mu$

It is also possible to express Ω in terms of the eigenstates of the Hamiltonian with some mathematical manipulation

$$\langle n' | H | n \rangle = \delta_{n'n} \to \partial_\mu \langle n' | H | n \rangle = 0$$

$$\partial_\mu \langle n' | H | n \rangle = \langle \partial_\mu n' | H | n \rangle + \langle n' | H | \partial_\mu n \rangle + \langle n' | \partial_\mu H | n \rangle$$

$$E_n \langle \partial_\mu n' | n \rangle + E_{n'} \langle n' | \partial_\mu n \rangle = \langle n' | \partial_\mu H | n \rangle$$

$$(E_{n'} - E_n) \langle n' | \partial_\mu n \rangle = \langle n' | \partial_\mu H | n \rangle$$

$$\langle n' | \partial_\mu n \rangle = \frac{\langle n' | \partial_\mu H | n \rangle}{E_{n'} - E_n} \tag{1.26}$$

Now we write equation 1.24 like so

$$\Omega^n_{\mu\nu} = i \langle \partial_\mu n | \partial_\nu n \rangle - (\mu \leftrightarrow \nu) = i \sum_{n' \neq n} \langle \partial_\mu n | n' \rangle \langle n' | \partial_\nu n \rangle - (\mu \leftrightarrow \nu)$$

By plugging in above equation 1.26 we get

$$\boxed{\Omega^n_{\mu\nu} = i \sum_{n' \neq n} \frac{\langle n | \partial_\mu H | n' \rangle \langle n' | \partial_\nu H | n \rangle}{(E_{n'} - E_n)^2} - (\mu \leftrightarrow \nu)} \tag{1.27}$$

This last form of the Berry curvature has the advantage that no differentiation of the wavefunction is needed. This equation also tells us that

$$\sum_n \Omega^n_{\mu\nu}(\boldsymbol{\lambda}) = 0$$

Equation 1.27 can also be written as

$$\boldsymbol{\Omega}^n = \sum_{n' \neq n} \frac{\langle n | \nabla H | n' \rangle \wedge \langle n' | \nabla H | n \rangle}{(E_{n'} - E_n)^2} \tag{1.28}$$

1.4   Stokes' Theorem

From the Stokes theorem we have that

$$\gamma_n = \oint_{\mathcal{P}} A^n_\mu \, d\lambda^\mu = \frac{1}{2} \int_\Sigma \Omega^n_{\mu\nu} \, d\lambda^\mu \wedge d\lambda^\nu \tag{1.29}$$

where we have used the Einstein convention of summation.

There is a subtelty in this last equation, as we know the Berry curvature tensor in Gauge-invariant, so the integral over the surface is too, but the integral over the closed path of the Berry connection is defined up to a factor $2n\pi$ that is gauge dependant. So is there a modulo 2π ambiguity or not?

The answer is that if γ_n is to be determined using the knowledge of $|n, \boldsymbol{\lambda}\rangle$

Figure 1.3: Here we divide the surface of the sphere in two different surfaces $\mathcal{A}$ and $\mathcal{B}$ that share the edge $\mathcal{P}$

only on the curve $\mathcal{P}$ then it is really well defined modulo 2π. In this case we can re-write equation 1.29 as

$$\frac{1}{2} \int_{\Sigma} \Omega^n_{\mu\nu} \, d\lambda^\mu \wedge d\lambda^\nu := \oint_{\mathcal{P}} A^n_\mu \, d\lambda^\mu$$

Meaning that the integral over the surface Σ is equal to *one of the values of the integrals along the closed path* $\mathcal{P}$

But what kind of Gauge gives the "correct" answer? If we choose a gauge that is continuous and smooth everywhere along the surface Σ including on its boundary $\mathcal{P}$ then equation 1.29 becomes unambiguous.

While it is possible to make a radical gauge transformation that shifts γ_n by 2π when regarding $|n, \boldsymbol{\lambda}\rangle$ as a function defined only in the neighborhood of $\mathcal{P}$, such a gauge change cannot be smoothly continued into the interior $\mathcal{S}$ without creating a vortex-like singularity of $\gamma_n(\boldsymbol{\lambda})$.

1.5   Chern Theorem

Let's take as an example Gauss's theorem. It tells us that the flux of the field through a closed surface is equal to the charges inside.

Now let's calculate the flux of the Berry curvature through a closed surface. We can divide the closed surface as two different open surfaces that share
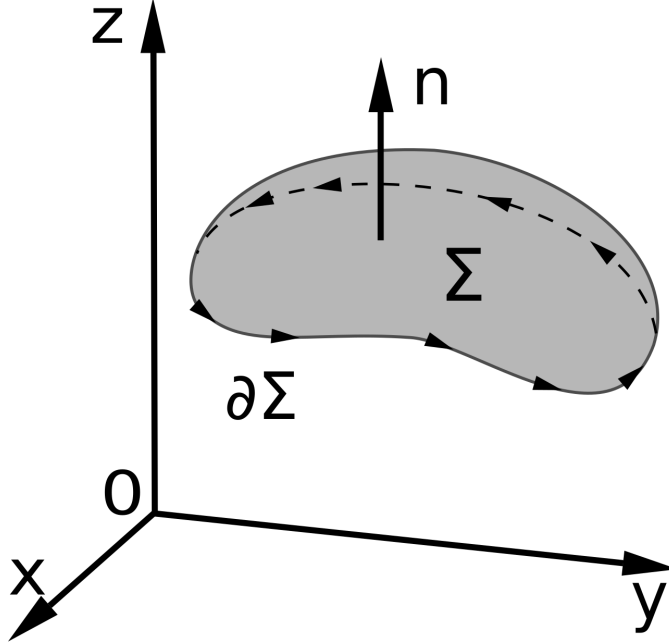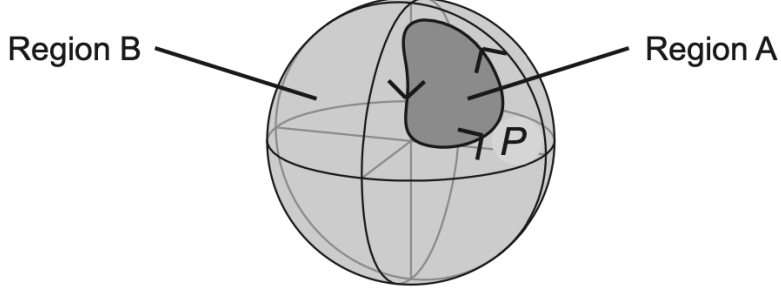
Figure 1.4: Here we divide the surface of the sphere in two different surfaces $\mathcal{A}$ and $\mathcal{B}$ that share the edge $\mathcal{P}$

the same edge $\mathcal{P}$.

Thanks to stokes theorem the flux through the surface $\mathcal{A}$ is $\oint_{\mathcal{P}} \mathbf{A} \cdot d\boldsymbol{\lambda}$, but the flux through the surface $\mathcal{B}$ is $-\oint_{\mathcal{P}} \mathbf{A} \cdot d\boldsymbol{\lambda}$.

Theese two integrals must be equal modulo 2π, so

$$\oint_{\mathcal{S}} \Omega_{\mu\nu}^n d\lambda^\mu \wedge d\lambda^\nu = 2\pi C_n \qquad C_n \in \mathbb{Z} \tag{1.30}$$

This means that the flux thought a closed surface of the Berry curvature is quantized

The constant C in known as the Chern number. Note that when the Chern index is nonzero, it is impossible to construct a smooth and continuous gauge over the entire surface $\mathcal{S}$. If such a gauge did exist, then we could apply Stokes' theorem directly to the entire surface and conclude that the Chern number vanishes, in contradiction with the assumption.

But what are these "pseudo-charges" inside the closed surface that generate the flux?

In E.M. a simple way to spot charges (or monopoles) is to look at the fields and see if as some point it diverges as $1/(\mathbf{r} - \mathbf{r_0})^2$. Let's take a look at $\Omega_{\mu\nu}$ (eq. 1.27) and see if we can spot anything similar [6]

$$\Omega_{\mu\nu}^n = i \sum_{n' \neq n} \frac{\langle n | \partial_\mu H | n' \rangle \wedge \langle n' | \partial_\nu H | n \rangle}{\underbrace{[E_{n'}(\boldsymbol{\lambda}) - E_n(\boldsymbol{\lambda})]^2}_{\substack{\text{what happens if for some } \boldsymbol{\lambda}=\boldsymbol{\lambda}_d \\ \text{the two energies are the same?}}}} \tag{1.31}$$

So, suppose that for some $\boldsymbol{\lambda} = \boldsymbol{\lambda}_d$ we have that $E_n(\boldsymbol{\lambda}_d) = E_m(\boldsymbol{\lambda}_d)$, now we expand the energies near $\boldsymbol{\lambda}_d$ at first order

$$\begin{cases} E_n(\boldsymbol{\lambda}) \approx E_n(\boldsymbol{\lambda}_d) + \partial_{\boldsymbol{\lambda}} E_n|_{\boldsymbol{\lambda}=\boldsymbol{\lambda}_d} \cdot (\boldsymbol{\lambda} - \boldsymbol{\lambda}_d) \\ E_m(\boldsymbol{\lambda}) \approx E_n(\boldsymbol{\lambda}_d) + \partial_{\boldsymbol{\lambda}} E_m|_{\boldsymbol{\lambda}=\boldsymbol{\lambda}_d} \cdot (\boldsymbol{\lambda} - \boldsymbol{\lambda}_d) \end{cases}$$

---

[6] In the equation below I expressed explicitly the $\boldsymbol{\lambda}$ dependence in the denominator and condensed the formula using the wedge product $\wedge$

This means that

$$E_n(\boldsymbol{\lambda}) - E_m(\boldsymbol{\lambda}) \approx \partial_{\boldsymbol{\lambda}}(E_n - E_m)|_{\boldsymbol{\lambda}=\boldsymbol{\lambda}_d} \cdot (\boldsymbol{\lambda} - \boldsymbol{\lambda}_d)$$

so the denominator of the berry curvature near $\boldsymbol{\lambda}_d$ goes like $1/(\boldsymbol{\lambda} - \boldsymbol{\lambda}_d)^2$. This means that there are "charges" or "monopoles" that induce the flux through the closed surface, and they are localized where 2 (or more) energy levels cross

1.6 Kubo Formula

We'll derive the Kubo formula for a general, multi-particle (or, if you prefer, single particle) Hamiltonian H_0 where the subscript 0 means that this is the unperturbed Hamiltonian before we apply an electric field. We denote the eigenstates of the Hamiltonian as $|m\rangle$ with $H_0 |m\rangle = E_m |m\rangle$.

$$H_0 = \sum_i \left[\frac{1}{2m} (\boldsymbol{p}_i - e\boldsymbol{A}_0)^2 + V_0(\boldsymbol{r}_i) \right] + \sum_{i \neq j} V_{ee}(\boldsymbol{r}_i - \boldsymbol{r}_j) \qquad (1.32)$$

Where $\boldsymbol{A}_0$ and V_0 are due to an existing EM field. Now we add a background electric field. We

$$H = \sum_i \left[\frac{1}{2m} (\boldsymbol{p}_i - e\boldsymbol{A}_0 - e\boldsymbol{A})^2 + V_0(\boldsymbol{r}_i) - e\boldsymbol{r}_i\phi(\boldsymbol{r}_i) \right] + \sum_{i \neq j} V_{ee}(\boldsymbol{r}_i - \boldsymbol{r}_j)$$
$$(1.33)$$

Which can be written as

$$H = H_0 + \sum_i -\frac{e}{m}\boldsymbol{\pi}_i \cdot \boldsymbol{A} - e\boldsymbol{r}_i\phi(\boldsymbol{r}_i) \qquad (1.34)$$

Where $\boldsymbol{\pi}_i = \boldsymbol{p} - e\boldsymbol{A}_0 = m\dot{\boldsymbol{r}}$ is the mechanical momentum, furthermore we can use the fact that the electric charge operator $\rho(\boldsymbol{r}) = -e \sum_i \delta(\boldsymbol{r} - \boldsymbol{r}_i)$ current operator $\boldsymbol{I}$ is equal to

$$\boldsymbol{I} = -e \sum_i \dot{\boldsymbol{r}}_i = -\sum_i \frac{e}{m}\boldsymbol{\pi}_i \qquad (1.35)$$

to re-write equation 1.34 like so

$$H = H_0 + \boldsymbol{I} \cdot \boldsymbol{A} + \int \rho(\boldsymbol{r})\phi(\boldsymbol{r})d\boldsymbol{r} \qquad (1.36)$$

however, we can assume that the density of charge ρ is always zero (it is usually considered when investigating dielectric properties of a material, but here we are interested in conduction, so we are ignoring it)

$$H(\boldsymbol{A}) = H_0 + \boldsymbol{I} \cdot \boldsymbol{A} \qquad (1.37)$$

At this point we need to write the perturbation in terms of the electric field, we can choose a gauge where $\boldsymbol{E} = -\partial_t \boldsymbol{A}$ and assume that the wave is monochromatic $\boldsymbol{E}(t) = \boldsymbol{E}e^{-i\omega t}$, so

$$A = \frac{\boldsymbol{E}}{i\omega}e^{i\omega t} \tag{1.38}$$

Our goal is to compute the current $\langle \boldsymbol{I} \rangle$ that flows due to the perturbation ΔH. To do so we'll work in the *interaction picture*, this means that the operators evolve as $\mathcal{O}(t) = V^{-1}\mathcal{O}V$ with $V = e^{-iH_0 t/\hbar}$. This means that the states evolve by

$$|\psi(t)\rangle = U(t, t_0)|\psi(t_0)\rangle\,; \quad U(t, t_0) = T\exp\left(-\frac{i}{\hbar}\int_{t_0}^{t}\Delta H(t')dt'\right) \tag{1.39}$$

Where T is the time ordering, keep in mind that since we are in the interaction picture $\Delta H(t) = V^{-1}\Delta H V$.

We now prepare the system at time $t = -\infty$ in a specific many body state $\rho_0 = \sum_i p_i |i\rangle \langle i|$ (it usually is either the ground state or a thermodynamic distribution). Keep in mind that the density operator, in the interaction picture evolves with the states

$$\begin{aligned}
\rho(t) &= \sum_i p_i |\psi_i(t)\rangle \langle \psi_i(t)| = \\
0 &= \sum_i p_i U(t, t_0)|\psi_i(t_0)\rangle \langle \psi_i(t_0)|U^{-1}(t, t_0) = \\
&= U(t, t_0)\rho(t_0)U^{-1}(t, t_0)
\end{aligned} \tag{1.40}$$

Then, writing $U(t) = T(t, t_0 \to -\infty)$, the expectation value of the current is

$$\begin{aligned}
\langle \boldsymbol{I}(t) \rangle &= \mathrm{tr}\left[\rho(t)\boldsymbol{I}(t)\right] = \\
&= \mathrm{tr}\left[U(t)\rho_0 U^{-1}(t)\boldsymbol{I}(t)\right] = \\
&= \mathrm{tr}\left[\rho_0 U^{-1}(t)\boldsymbol{I}(t)U(t)\right] = \\
&= \langle U^{-1}(t)\boldsymbol{I}(t)U(t)\rangle_0 \approx \\
&\approx \langle \boldsymbol{I}(t)\rangle_0 + \left\langle \frac{i}{\hbar}\int_{-\infty}^{t}[\Delta H(t'), \boldsymbol{I}(t)]dt'\right\rangle_0
\end{aligned} \tag{1.41}$$

Where in the last passage we've expanded the exponential in the U operator (equation 1.39), and $\langle \dots \rangle_0$ means the average with respect to ρ_0. The first term is the current in the absence of an electric field, therefore it is zero. Using equation 1.37 and 1.38 and plugging it in the last equation we have that the current due to the electric field is then

$$\langle I_i(t) \rangle = \frac{1}{\hbar\omega}\int_{\infty}^{t}\langle [I_j(t'), I_i(t)]\rangle_0 E_j e^{-i\omega t'}dt' \tag{1.42}$$

Because the system is invariant under time translations, the correlation function above can bony depend on $t'' = t - t'$, we can rewrite the expression above as

$$\frac{E_j e^{-i\omega t}}{\hbar\omega} \int_0^\infty e^{i\omega t''} \langle [I_j(0), I_i(t'')]\rangle_0 dt'' \tag{1.43}$$

. The only t dependence in the formula above sits outside as $e^{-i\omega t}$. This means that the proportionality constant is the conductance. To get the conductivity σ (conductance per unit area, we just have to divide the surface S), and the off diagonal part is the *Hall conductivity*

$$\sigma_{xy} = \frac{1}{S\hbar\omega} \int_0^\infty e^{i\omega t} \langle [I_x(0), I_y(t)]\rangle_0 dt \tag{1.44}$$

This is the *Kubo formula* for the Hall conductivity.

1.7   Quantization of Hall conductivity

Our job here is not done, we got Kubo formula the Hall conductivity 1.44, but to capture the most important property we need to do some mathematical manipulation. Using the fact hat $\boldsymbol{I}(t) = V^{-1}\boldsymbol{I}(0)V$ with $V = e^{-iH_0 t/\hbar}$ we can write

$$\sigma_{xy}(\omega) = \frac{1}{S\hbar\omega} \int_0^\infty e^{i\omega t} \sum_{nm} p_n \left[\langle n|I_y|m\rangle \langle m|I_x|n\rangle e^{-iE_{nm}t/\hbar} - (n \leftrightarrow m) \right] dt$$

Now we can perform the integral in dt, since the states with $n = m$ cancel out we have that

$$\sigma_{xy}(\omega) = -\frac{i}{\omega S} \sum_{nm} p_n \left[\frac{\langle n|I_y|m\rangle \langle m|I_x|n\rangle}{\hbar\omega - E_{nm}} - (n \leftrightarrow m) \right] \tag{1.45}$$

To get the Hall conductivity for DC current we have to evaluate $\sigma_{xy}(\omega \to 0)$, in this limit

$$\lim_{\omega \to 0} \frac{1}{\hbar\omega - E_{nm}} = -\frac{1}{E_{nm}} + \frac{\hbar\omega}{(E_{nm})^2}$$

Plugging the zeroth-order we get

$$\begin{aligned} \sigma_{xy} &= \frac{i}{\omega S} \sum_{nm} p_n \left[\frac{\langle n|I_y|m\rangle \langle m|I_x|n\rangle}{E_{nm}} - (n \leftrightarrow m) \right] = \\ &= \frac{i}{\omega S} \sum_{nm} \frac{p_n}{E_{nm}} \left[\langle n|I_y|m\rangle \langle m|I_x|n\rangle + (n \leftrightarrow m) \right] = \\ &= 0 \end{aligned} \tag{1.46}$$

That is equal to zero because the terms inside the summation are asymmetric under the exchange of $(n \leftrightarrow m)$, and we are summing over all the possible n

and m. For the first order term we have

$$\sigma_{xy} = \frac{i\hbar}{S} \sum_{nm} \frac{p_n}{(E_{nm})^2} \left[\langle n|I_y|m \rangle \langle m|I_x|n \rangle - (n \leftrightarrow m) \right] \qquad (1.47)$$

From equation 1.37 we can see that $I_i = \partial H / \partial A_i$, this means that the equation above becomes

$$
\begin{aligned}
\sigma_{xy} =& \frac{i\hbar}{S} \sum_{nm} \frac{p_n}{(E_{nm})^2} \left[\langle n|I_y|m \rangle \langle m|I_x|n \rangle - (n \leftrightarrow m) \right] = \\
=& \frac{\hbar}{S} \sum_n p_n \sum_{m \neq n} \frac{i}{(E_{nm})^2} \left[\left\langle n \left| \frac{\partial H}{\partial A_y} \right| m \right\rangle \left\langle m \left| \frac{\partial H}{\partial A_x} \right| n \right\rangle - (n \leftrightarrow m) \right] = \\
=& \frac{\hbar}{S} \sum_n p_n \Omega^n_{A_x A_y}
\end{aligned}
$$
$$(1.48)$$

This is a nice formula, however it doesn't explain why σ_{xy} is quantized, however if we average over all possible values of $\boldsymbol{A}$, which comes from all the possible value of the fluxes

$$
\begin{aligned}
\langle \sigma_{xy} \rangle =& \frac{\int \sigma_{xy} d^2 \boldsymbol{A}}{\int d^2 \boldsymbol{A}} = \\
=& \left(\frac{S}{\Phi_0^2} \right) \frac{\hbar}{S} \sum_n p_n \int \Omega^n_{A_x A_y} d^2 \boldsymbol{A} = \\
=& \left(\frac{e^2}{4\pi^2 \hbar^2} \right) 2\pi\hbar \sum_n p_n C_n = \\
=& \frac{e^2}{2\pi\hbar} \sum_n p_n C_n \qquad \text{with } C_n \in \mathbb{Z}
\end{aligned}
$$
$$(1.49)$$

Where we have defined the Chern numbers $2\pi C_n = \int \Omega^n_{A_x A_y} d^2 \boldsymbol{A}$ and for the Stokes theorem it is a multiple of 1. The most emblematic passage here is why $\int d^2 \boldsymbol{A} = \Phi_0^2 / S$.

σ_{xy} at low temperatures

In equation 1.49 we had a contribution that is the average of C_n over all the states, if we are at low temperature there are two possibilities depending on the treatment we had on the wavefunction

- **Many body interacting wavefunction** For $T \to 0$ we have that it will be at the fundamental state $p_0 \to 1$ and $p_i \to 0$ for $i \neq 0$, this means that $\sum_n p_n C_n \to C_0$, therefore a quantized conductivity quill be observed

- **Non-interacting single particle wavefunctions** For $T \to 0$ the electrons will settle in a Fermi-Dirac distribution, so

$$\sum_n p_n C_n = N^{-1} \sum_n C_n \theta(E_F - E_n)$$

where N is the total number of electrons and E_F is the Fermi energy. Although it's not as easy to prove that is generally quantized due to the N^{-1} factor,[7] we'll see that it's much easier to calculate the precise value for real world scenarios, and it's going to be the subject of the next section

1.8 Berry phase in Bloch bands

The band structure of crystals provides a natural platform to investigate the occurrence of the berry phase effect. Within the independent electron approximation, the band structure of a crystal is determined by the Bloch Hamiltonian:

$$H = \frac{\boldsymbol{p}^2}{2m} + V(\boldsymbol{r}) \tag{1.50}$$

Where $V(\boldsymbol{r} + \boldsymbol{a}) = V(\boldsymbol{r})$ is the periodic potential with a being the Bravais lattice vector. According to Bloch's theorem the eigenstates satisfy

$$\psi_{n\boldsymbol{k}}(\boldsymbol{r} + \boldsymbol{a}) = e^{i\boldsymbol{k}\cdot\boldsymbol{a}}\psi_{n\boldsymbol{k}}(\boldsymbol{r}) \tag{1.51}$$

where n is the band index and $\hbar\boldsymbol{k}$ is the crystal momentum. To comply with the general formalism of the Berry phase, we make the following unitary transformation to obtain a $\boldsymbol{k}$-dependent Hamiltonian

$$e^{-i\boldsymbol{k}\cdot\boldsymbol{r}} H e^{i\boldsymbol{k}\cdot\boldsymbol{r}} = H = \frac{(\boldsymbol{p} + \hbar\boldsymbol{k})^2}{2m} + V(\boldsymbol{r}) \tag{1.52}$$

The transformed eigenstate $u_{n\boldsymbol{k}}(\boldsymbol{r}) = e^{-i\boldsymbol{k}\cdot\boldsymbol{r}}\psi_{n\boldsymbol{k}}(\boldsymbol{r})$ is just the cell-periodic part of the Bloch function. It satisfies the strict periodic boundary condition

$$u_{n\boldsymbol{k}}(\boldsymbol{r} + \boldsymbol{a}) = u_{n\boldsymbol{k}}(\boldsymbol{r}) \tag{1.53}$$

We can now identify the Brillouin zone as the parameter space of the transformed Hamiltonian $H(\boldsymbol{k})$, and $u_{n\boldsymbol{k}} = |n, \boldsymbol{k}\rangle$ as the basis function.
In this regime the Kubo formula 1.47 becomes

$$\sigma_{xy} = i\hbar \sum_{m, E_n < E_F} \int_{T^2} \frac{\langle n, \boldsymbol{k}|J_y|m, \boldsymbol{k}\rangle \langle m, \boldsymbol{k}|J_x|n, \boldsymbol{k}\rangle - (n \leftrightarrow m)}{E_m(\boldsymbol{k}) - E_n(\boldsymbol{k})} \frac{d^2\boldsymbol{k}}{(2\pi)^2} \tag{1.54}$$

---

[7]Even thought we know for sure it must be quantized, because we can always reparametrize Non-interacting single particle wavefunctions into many body interacting wavefunction

And it is called the TKNN formula [3]

We can define the current in terms of the group velocity of the wavepackets

$$\boldsymbol{J} = \frac{e}{\hbar} \frac{\partial H}{\partial \boldsymbol{k}} \tag{1.55}$$

this means that equation 1.54 is equal to

$$\sigma_{xy} = \frac{e^2}{\hbar} \sum_{E_n < E_F} \Omega^n_{k_x k_y} \frac{d^2 \boldsymbol{k}}{(2\pi)^2} \tag{1.56}$$

Using the Chern theorem 1.30 we have that the equation above is equal to

$$\frac{e^2}{2\pi\hbar} \sum_n^N C_n \tag{1.57}$$

where C_n is the Chern number of the n-th band and the bands up to the N-th band are occupied, therefore we sum over the occupied bands

1.9   Graphene

Graphene is a two-dimensional lattice of carbon atoms, arranged in a honeycomb structure as shown in the figure 1.5 Although it is straightforward to build many layers of these lattices (a substance known as graphite), it was long thought that a purely two-dimensional lattice would be unstable to thermal fluctuations and impossible to create. This changed in 2004 when Andre Geim and Konstantin Novoselov succeeded in isolating two-dimensional graphene [4]. For this, they won the 2010 Nobel prize. As we now show, the band structure of graphene is particularly interesting.

We define the primitive lattice vectors $\boldsymbol{a}_1$ and $\boldsymbol{a}_2$ as follows:

$$\boldsymbol{a}_1 = \frac{a}{2} \begin{bmatrix} 3 \\ \sqrt{3} \end{bmatrix} \qquad \boldsymbol{a}_2 = \frac{a}{2} \begin{bmatrix} 3 \\ -\sqrt{3} \end{bmatrix} \tag{1.58}$$

Where a is the distance between two neighboring atoms, which in graphene is $\approx 1.4 \times 10^{-10}$m. The sublattice A is defined as all the points $\boldsymbol{r} = n_1 \boldsymbol{a}_1 + n_2 \boldsymbol{a}_2$ with $n_i \in \mathbb{Z}$ (yellow points in figure 1.5), sublattice B is defined as all points $\boldsymbol{r} = n_1 \boldsymbol{a}_1 + n_2 \boldsymbol{a}_2 + \boldsymbol{\delta}$ with $\boldsymbol{\delta} = (a, 0)$ (blue points in figure 1.5).

The reciprocal lattice vectors $\boldsymbol{b}_i$ are the vectors that satisfy $\boldsymbol{a}_i \cdot \boldsymbol{b}_j = \delta_{ij}$ and are equal to

$$\boldsymbol{b}_1 = \frac{2\pi}{3a} \begin{bmatrix} 1 \\ \sqrt{3} \end{bmatrix} \qquad \boldsymbol{b}_2 = \frac{2\pi}{3a} \begin{bmatrix} 1 \\ -\sqrt{3} \end{bmatrix} \tag{1.59}$$

This reciprocal lattice is also triangular. The Brillouin zone is constructed in the usual manner by drawing perpendicular boundaries between the origin
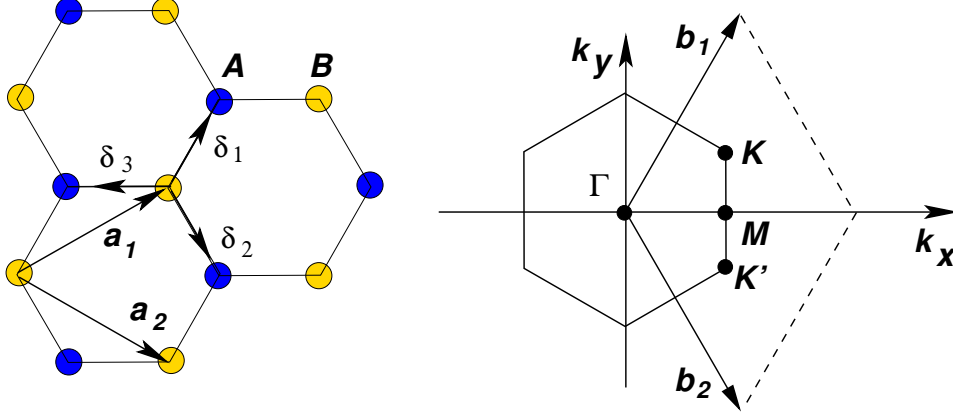
Figure 1.5: On the left there is the lattice structure of graphene made out of two interpenetrating triangular lattices (a_1 and a_2 are the lattice unit vectors, and δ_i with $i \in 1, 2, 3$ are the nearest neighbors. On the right the corresponding Brillouin zone, the Dirac cones are located at the K_0 and K_1 points) [5]

and each other point in the reciprocal lattice giving rise to a hexagonal Brillouin zone with $\boldsymbol{K}_0$ and $\boldsymbol{K}_1$ as the vertices of the hexagon, where

$$\boldsymbol{K}_0 = \frac{1}{3}(2\boldsymbol{b}_1 + \boldsymbol{b}_2) \qquad \boldsymbol{K}_1 = \frac{1}{3}(\boldsymbol{b}_1 + 2\boldsymbol{b}_2)$$

$$\boldsymbol{K}_0 = \frac{2\pi}{3a}\left(1, \frac{1}{\sqrt{3}}\right) \qquad \boldsymbol{K}_1 = \frac{2\pi}{3a}\left(1, -\frac{1}{\sqrt{3}}\right) \tag{1.60}$$

The tight binding approach

To investigate the band structure of graphene, we are going to use the tight binding approach [6, 7]. First we write the Hamiltonian.

$$H = \frac{\boldsymbol{p}^2}{2m} + \sum_{\boldsymbol{R} \in C} V_a(x - \boldsymbol{R}) \tag{1.61}$$

Where V_a is the potential of the single carbon atom, the set
$C = \{n_1\boldsymbol{a}_1 + n_2\boldsymbol{a}_2 + \nu\boldsymbol{\delta} \,|\, n_1, n_2 \in \mathbb{Z}, \nu \in \{0,1\}\}$ is the set of all the positions of the atoms.
We can re-write the potential of the Hamiltonian in this more convenient manner.

$$\sum_{\boldsymbol{R} \in C} V_a(x - \boldsymbol{R}) = V_a(x) + V'(x) \tag{1.62}$$

Where $V'(x)$ the potential of the other atoms, this way the can be divided in two parts:

$$H = \underbrace{\frac{\boldsymbol{p}^2}{2m} + V_a(x)}_{\substack{\text{single-atom} \\ \text{Hamiltonian}}} + \underbrace{V'(x)}_{\text{perturbation}} \tag{1.63}$$

Let $|n, \boldsymbol{R}\rangle$ be the n-th eingenstate of the Hamiltonian of single carbon atom placed in $\boldsymbol{R}$. Due to translational symmetry, the wave function must satisfy the Bloch theorem, this tells us that the eingenstates of the Hamiltonian can be written as

$$|n, \nu, \boldsymbol{k}\rangle = \sum_{\boldsymbol{R}_\nu \in C_\nu} e^{i\boldsymbol{k}\cdot\boldsymbol{R}_\nu} |n, \boldsymbol{R}_\nu\rangle \qquad (1.64)$$

with $\nu \in \{0, 1\}$ and C_ν si defined as

$$C_\nu = \{n_1\boldsymbol{a}_1 + n_2\boldsymbol{a}_2 + \nu\boldsymbol{\delta} \,|\, n_1, n_2 \in \mathbb{Z}\}$$

With this we can now calculate the matrix elements of the Hamiltonian

$$\langle n, \nu, \boldsymbol{k}|H|n', \nu', \boldsymbol{k}'\rangle = \sum_{\boldsymbol{k}\boldsymbol{k}', \boldsymbol{R}\boldsymbol{R}'} e^{i\boldsymbol{k}\cdot(\boldsymbol{R}+\nu\boldsymbol{\delta})-i\boldsymbol{k}'\cdot(\boldsymbol{R}+\nu'\boldsymbol{\delta})}\langle n, \nu, \boldsymbol{R}|H|n', \nu', \boldsymbol{R}'\rangle \tag*{(1.65)}$$

Since the matrix elements inside the summation don't depend on k we have that the terms with $k \neq k'$ are equal to zero. So the equation above becomes

$$\langle n, \nu, \boldsymbol{k}|H|n', \nu', \boldsymbol{k}'\rangle = \langle n, \nu, \boldsymbol{k}|H|n', \nu', \boldsymbol{k}\rangle\delta_{\boldsymbol{k},\boldsymbol{k}'}$$

This means that

$$\langle n, \nu, \boldsymbol{k}|H|n', \nu', \boldsymbol{k}\rangle = \sum_{\boldsymbol{k}, \boldsymbol{R}\boldsymbol{R}'} e^{i\boldsymbol{k}\cdot(\boldsymbol{R}-\boldsymbol{R}'+\nu\boldsymbol{\delta}-\nu'\boldsymbol{\delta})}\langle n, \nu, \boldsymbol{R}|H|n', \nu', \boldsymbol{R}'\rangle$$

And, since it only depends on $\boldsymbol{R} - \boldsymbol{R}'$ we have that

$$\langle n, \nu, \boldsymbol{k}|H|n', \nu', \boldsymbol{k}\rangle = \sum_{\boldsymbol{k}, \boldsymbol{R}} e^{i\boldsymbol{k}\cdot\boldsymbol{R}+i(\nu-\nu')\boldsymbol{k}\cdot\boldsymbol{\delta}}\langle n, \nu, \boldsymbol{R}|H|n', \nu', \boldsymbol{0}\rangle \qquad (1.66)$$

Now we need to calculate the matrix elements $\langle n, \nu, \boldsymbol{R}|H|n', \nu', \boldsymbol{0}\rangle$. Using equation 1.63 we get that if $\boldsymbol{R} = \boldsymbol{0}$

$$\langle n, \nu, \boldsymbol{0}|H|n', \nu', \boldsymbol{0}\rangle = E_n\langle n, \nu, \boldsymbol{0}|n', \nu', \boldsymbol{0}\rangle + \langle n, \nu, \boldsymbol{0}|V'(\boldsymbol{r})|n', \nu', \boldsymbol{0}\rangle \quad (1.67)$$

For $\nu = \nu'$ the first term $(E_n\langle n, \nu, \boldsymbol{0}|n', \nu, \boldsymbol{0}\rangle = \delta_{nn'})$ and the second term, which is called crystal field integral is usually neglected because in most cases they simply produce a rigid shift of the energy bands $E_n(\boldsymbol{k})$ without affecting their dispersion. [8]

For $\nu \neq \nu'$ the second term is much bigger than the first one, so

$$\langle n, \nu, \boldsymbol{0}|H|n', \nu', \boldsymbol{0}\rangle \approx E_n\delta_{nn'}\delta_{\nu\nu'} + \langle n, \nu, \boldsymbol{0}|V'(\boldsymbol{r})|n', \nu', \boldsymbol{0}\rangle(1 - \delta_{\nu\nu'}) \quad (1.68)$$

Since we consider the wavefunctions as strongly localized, the second term is much smaller than the first one, so we can ignore it.

Usually the matrix elements $\langle n, \nu, \boldsymbol{0}|V'(\boldsymbol{r})|n', \nu', \boldsymbol{0}\rangle$ are conveniently expressed

$$\langle\, s\,, \nu, \mathbf{0}|V'(\mathbf{r})\,|\, s\,, \nu', \mathbf{0}\rangle = V(ss\sigma)$$

$$\langle\, s\,, \nu, \mathbf{0}|V'(\mathbf{r})\,|p_x, \nu', \mathbf{0}\rangle = l_x V(sp\sigma)$$

$$\langle p_x, \nu, \mathbf{0}|V'(\mathbf{r})\,|p_x, \nu', \mathbf{0}\rangle = l_x^2 V(pp\sigma) + (1 - l_x^2)V(pp\pi)$$

$$\langle p_x, \nu, \mathbf{0}|V'(\mathbf{r})\,|p_y, \nu', \mathbf{0}\rangle = l_x l_y \left[V(pp\sigma) - V(pp\pi)\right]$$

$$\langle p_x, \nu, \mathbf{0}|V'(\mathbf{r})\,|p_z, \nu', \mathbf{0}\rangle = l_x l_z \left[V(pp\sigma) - V(pp\pi)\right]$$

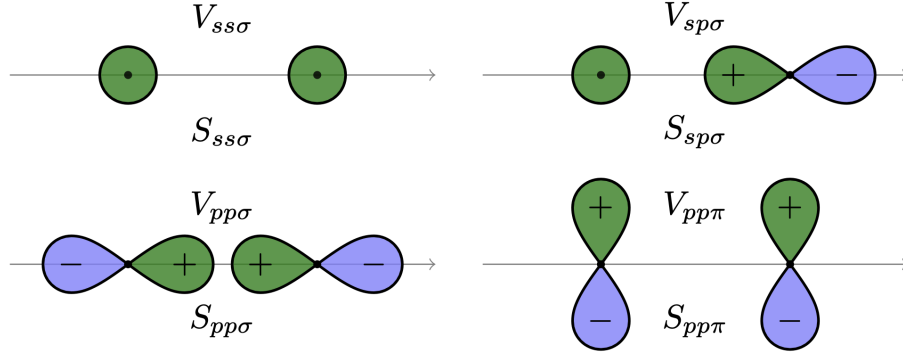**Table 1.1:** Here we have defined $\boldsymbol{\delta} = (l_x, l_y, l_z)|\delta|$

Figure 1.6: Each one of the potentials $V(ss\sigma), V(sp\sigma), V(pp\sigma), V(pp\pi)$ represent a different kind of bonding between the two orbitals. The first two indices represent the orbitals (s and p), the last one represent the bonding type (σ and π)

in terms of a a small number of independent parameters, and are evaluated either analytically, or numerically, or semi-empirically.

In the case of carbon atoms we only need to work with atomic orbitals of type s and p, this means that the independent matrix elements to evaluate are shown in table **??**

These parameters can be pictorially shown in figure 1.6

The Hamiltonian matrix should be a 8×8 matrix. Nevertheless, from group theory we know that at a general point k the Bloch functions derived from s, p_x and p_y atomic functions never mix with the Bloch function p_z because of the symmetry operation of reflection through the xy plane. We can thus classify the energy states as even or odd with respect to this transformation; the former give rise to the so-called σ-bands and the latter to the so-called π-bands. Moreover, the problem is decomposed into two decoupled sub-problems and, instead of diagonalizing a single 8×8 matrix, we have to cope separately with a 2×2 matrix (π-bands) and a 6×6 matrix (σ-bands). Fortunately the σ-bands are fully below the Fermi-level, so they don't have

any contribution to the electron-transport phenomenon, so we only have to deal with the 2×2 matrix of the π-bands

$$\langle p_z, \nu, \mathbf{0}|H|p_z, \nu', \mathbf{0}\rangle = \begin{bmatrix} E_p & V(pp\pi) \\ V(pp\pi) & E_p \end{bmatrix} \tag{1.69}$$

Now we can evaluate equation 1.66 considering just the nearest-neighbors

$$\langle p_z, 0, \mathbf{k}|H|p_z, 0, \mathbf{k}\rangle = \sum_{\mathbf{k}, \mathbf{R}} e^{i\mathbf{k}\cdot\mathbf{R}} \langle p_z, 0, \mathbf{R}|H|p_z, 0, \mathbf{0}\rangle \approx E_p \tag{1.70}$$

$$\langle p_z, 0, \mathbf{k}|H|p_z, 1, \mathbf{k}\rangle = \sum_{\mathbf{k}, \mathbf{R}} e^{i\mathbf{k}\cdot\mathbf{R}+i\mathbf{k}\cdot\boldsymbol{\delta}} \langle p_z, 0, \mathbf{R}|H|p_z, 1, \mathbf{0}\rangle \approx$$

$$\approx \sum_i e^{i\mathbf{k}\cdot\boldsymbol{\delta}_i} V(pp\pi) \equiv \tag{1.71}$$

$$\equiv V(pp\pi)F(\mathbf{k})$$

Where $F(\mathbf{k})$ is defined as the geometrical form factor, and it is equal to

$$F(\mathbf{k}) = \sum_{\boldsymbol{\delta}_i} e^{i\mathbf{k}\cdot\boldsymbol{\delta}_i} = 1 + 2\cos\frac{k_x\delta}{2} e^{-i\frac{\sqrt{3}}{2}k_y\delta} \tag{1.72}$$

Therefore, the k-dependent Hamiltonian for the π-bands is

$$\langle p_z, \nu, \mathbf{k}|H|p_z, \nu', \mathbf{k}'\rangle = \delta_{kk'} \begin{bmatrix} E_p & V(pp\pi)F(\mathbf{k}) \\ V(pp\pi)F(\mathbf{k}) & E_p \end{bmatrix} \tag{1.73}$$

However before diagonalizing the Hamiltonian we have to keep in mind that we don't start off with an orthonormal base of states

$$\langle p_z, \nu, \mathbf{k}|p_z, \nu', \mathbf{k}\rangle \equiv S_{\nu\nu'}(\mathbf{k}) = \begin{bmatrix} 1 & sF(\mathbf{k}) \\ sF(\mathbf{k}) & 1 \end{bmatrix} \tag{1.74}$$

This means that the eigenvalue equation is

$$\det|H_{\nu\nu'}(\mathbf{k}) - E(\mathbf{k})S_{\nu\nu'}(\mathbf{k})| = 0 \tag{1.75}$$

The eigenvalues of the Hamiltonian gives us the dispersion relation 1.7

$$E(\mathbf{k}) = \frac{E_p \pm V(pp\pi)|F(\mathbf{k})|}{1 \mp s|F(\mathbf{k})|} \tag{1.76}$$

Near the degenerate points $\mathbf{K}_0$ and $\mathbf{K}_1$ (eq. 1.60), the geometrical form factor can be expanded in Taylor series to first order in the wavevector
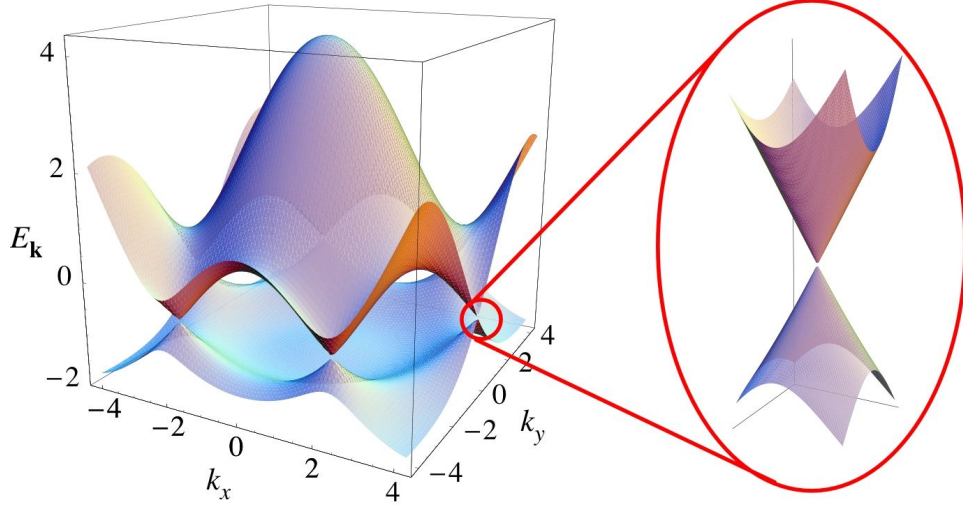
24

Figure 1.7: This is the dispersion relation for the single layer graphene, notice how near the vertices of the reciprocal lattice we get a cone-like dispersion relation typical of relativistic massless particles [5]

measured from the $\boldsymbol{K}_0$ and $\boldsymbol{K}_1$ points. The resulting expression of the form factors are

$$F_{\boldsymbol{K}_0}(\boldsymbol{k}) = -F^*_{\boldsymbol{K}_1}(\boldsymbol{k}) = -\frac{\sqrt{3}}{2}\delta(k_x - ik_y) \qquad (1.77)$$

This means that the matrix Hamiltonians near the degeneracies can be recast in the form

$$H_{\boldsymbol{K}_0}(\boldsymbol{k}) = -H^*_{\boldsymbol{K}_1}(\boldsymbol{k}) = \begin{bmatrix} 0 & v_F\hbar(k_x - ik_y) \\ v_F\hbar(k_x + ik_y) & 0 \end{bmatrix}; \quad v_f = \frac{\sqrt{3}}{2}\frac{\delta}{\hbar}V(pp\pi)$$
$$(1.78)$$

The eigenvalues of both Hamiltonians are

$$E(k) = \pm v_F\hbar k \quad \text{with} \quad k = \sqrt{k_x^2 + k_y^2} \qquad (1.79)$$

This means that electrons near the Dirac cones behave pretty much like photons, except that they move at the Fermi speed v_F instead of the speed of light.

The eigenstates of this Hamiltonian are called *Dirac-fermions* and are equal To

$$|\pm, \boldsymbol{k}\rangle = \frac{1}{\sqrt{2}}\begin{bmatrix} e^{-i\lambda\theta} \\ \pm e^{i\lambda\theta} \end{bmatrix}; \quad \theta = \arctan(k_x/k_y) \qquad (1.80)$$

where $\lambda = 1$ in K_0 and $\lambda = -1$ in K_1. Hence, the low-energy quasiparticles in graphene can be interpreted as Massless Dirac Fermion, and described by

a spinor wave function in which the spin degree-of-freedom is substituted with a sublattice degree-of-freedom, that is defined as *pseudospin*. We can also go futher on this, since an electron can be in a superposition between the two cones we can add an additional spin-like degree of freedom. The Hamiltonian 1.78 becomes

$$H(\boldsymbol{k}) = \hbar v_{\mathrm{F}}(\sigma_x \tau_z k_x + \sigma_y) \qquad (1.81)$$

Here $\boldsymbol{\sigma}$ and $\boldsymbol{\tau}$ are Pauli matrices with $\sigma_z = \pm 1$ describing states on the $A(B)$ sublattice and $\tau_z = \pm 1$ describing states at the $\boldsymbol{K}_0(\boldsymbol{K}_1)$ points.

1.10 Gapped Graphene

The reason why the dispersion relation of graphene is degenerate in the K points is due to the sub-lattice symmetry of the system. This means that for materials that don't have this symmetry such as Boron Nitrite exhibit an open gap in the K points, alternatively one could layer graphene on top of another honeycomb lattice that doesn't have sublattice symmetry, therefore subjecting it with a periodic potential that breaks the symmetry and opens the gap.

Mathematically speaking, the tight binding Hamiltonian has two different energies for the two different atoms in the sub-lattice. With respect to equation 1.78 it becomes

$$H_{\boldsymbol{K}_0}(\boldsymbol{k}) = -H^*_{\boldsymbol{K}_1}(\boldsymbol{k}) = \begin{bmatrix} \Delta & v_F \hbar (k_x - ik_y) \\ v_F \hbar (k_x + ik_y) & -\Delta \end{bmatrix} \qquad (1.82)$$

Where Δ is half the difference of the diagonal energy on the two sublattices, and the energy zero has been shifted at the center of the energy gap. The dispersion relation now becomes

$$E(\boldsymbol{k}) = \pm \sqrt{\Delta^2 + (v_F \hbar k)^2} \qquad (1.83)$$

It is seen that the above dispersion curves are formally the same produced by the Dira equations, with the light velocity c replaced by the Fermi velocity v_F and the rest mass $m_0 = \Delta / v_F^2$

1.11 Bilayer graphene

In the tight-binding description of bilayer graphene, we take into account $2p_z$ orbitals on the four atomic sites in the unit cell, labelled as $j = A_1, B_1, A_2, B_2$. Then, the transfer integral matrix of bilayer graphene is a 4×4 matrix given by [9]
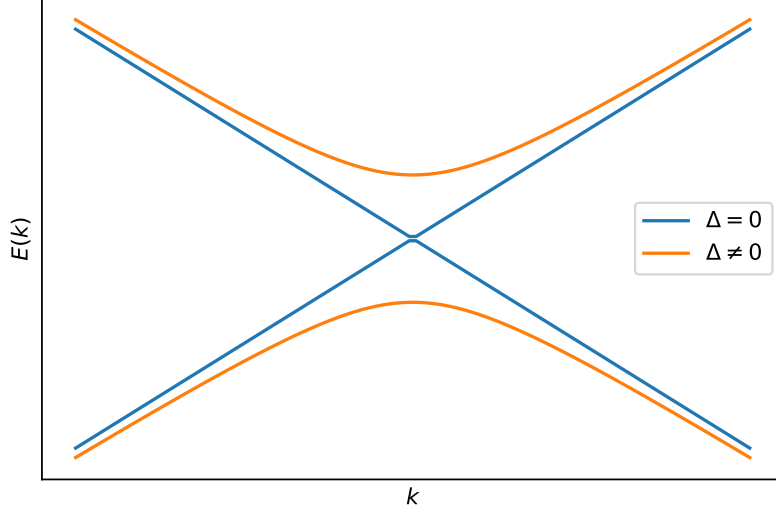
Figure 1.8: difference between the gapless and the gapped Dirac dispersion relation

$$
H(\boldsymbol{k}) =
\begin{bmatrix}
E_{A_1} & -\gamma_0 F(\boldsymbol{k}) & \gamma_4 F(\boldsymbol{k}) & -\gamma_3 F(\boldsymbol{k}) \\
-\gamma_0 F(\boldsymbol{k}) & E_{B_1} & -\gamma_1 & \gamma_4 F(\boldsymbol{k}) \\
\gamma_4 F(\boldsymbol{k}) & \gamma_1 & E_{A_2} & -\gamma_0 F(\boldsymbol{k}) \\
-\gamma_3 F(\boldsymbol{k}) & \gamma_4 F(\boldsymbol{k}) & -\gamma_0 F(\boldsymbol{k}) & E_{B_2}
\end{bmatrix}
\tag{1.84}
$$

where the tight-binding parameters are defined as

$$
\begin{aligned}
\gamma_0 &= -\langle A_1|H|B_1\rangle = -\langle A_2|H|B_2\rangle \\
\gamma_1 &= \langle A_2|H|B_1\rangle \\
\gamma_3 &= -\langle A_1|H|B_2\rangle \\
\gamma_4 &= \langle A_1|H|A_2\rangle = \langle B_1|H|B_2\rangle
\end{aligned}
\tag{1.85}
$$

The upper-right and lower-left square 2×2 blocks of H describe inter-layer coupling. Parameter γ_1 describes coupling between pairs of orbitals on sites that are directly above each other B_1 and A_2 (also called dimer sites): since this is a vertical coupling, the corresponding terms in H do not contain $F(\boldsymbol{k})$ which describes in-plane hopping. The other γ factors do have an in plane component, which causes the $F(\boldsymbol{k})$ term to show up.

(a)

(b)

Figure 1.9: Schematic representation of the bilayer graphene structure

Parameter	Value [eV]
γ_0	3.16 ± 0.03
γ_1	0.381 ± 0.003
γ_3	0.38 ± 0.06
γ_4	0.14 ± 0.03
s_0	boh
s_1	boh

Table 1.2: Values in eV of γ_i [10]

The overlap matrix S form equation 1.74 becomes in the bilayer case

$$
S = \begin{bmatrix}
1 & s_0 F(\boldsymbol{k}) & 0 & 0 \\
s_0 F(\boldsymbol{k}) & 1 & s_1 & 0 \\
0 & s_1 & 1 & s_0 F(\boldsymbol{k}) \\
0 & 0 & s_0 F(\boldsymbol{k}) & 1
\end{bmatrix}
\tag{1.86}
$$

Here we only include two parameters: $s_0 = \langle A_1 | B_1 \rangle = \langle A_2 | B_2 \rangle$ describing non-orthogonality of intra-layer nearest-neighbours and $s_1 = \langle A_2 | B_1 \rangle$ describing non-orthogonality of orbitals on dimer sites A1 and B2. In principle, it is possible to introduce additional parameters analogous to γ_3, γ_4, etc., but generally they will be small and irrelevant, infact in the bilayer case it is common practice to neglect completely the overlap matrix if we are dealing with. The resulting energy bands are plotted in figure 1.10

To describe the properties of the electrons near the K we just have to approximate $F(\boldsymbol{k})$ just like we did in equation 1.77. This results in a Hamiltonian that is the generalization of the one we had in equation 1.82

$$
H_{\boldsymbol{K}_0} = -H_{\boldsymbol{K}_1}^* = \begin{bmatrix}
E_{A_1} & v_F \pi^\dagger & -v_4 \pi^\dagger & v_3 \pi \\
v_F \pi & E_{B_1} & \gamma_1 & -v_4 \pi^\dagger \\
-v_4 \pi & \gamma_1 & E_{A_2} & v_F \pi^\dagger \\
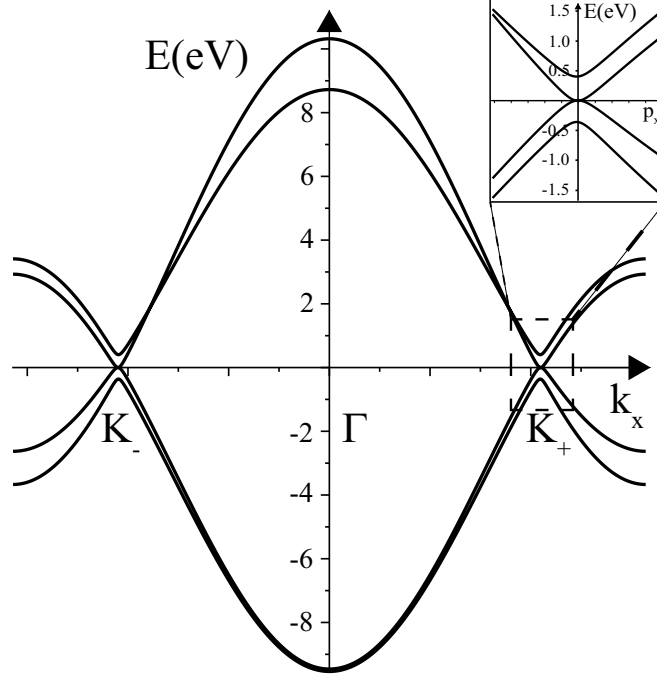v_3 \pi^\dagger & -v_4 \pi & v_F \pi & E_{B_2}
\end{bmatrix}
\tag{1.87}
$$

Figure 1.10: Here are plotted the p_z orbitals along the k_x axis in the recipro-
cal space intersecting the corners K_0 and K_1 and the center Γ of the Brillouin
zone. Notice how now we have four bands, this because we have four atoms in the
fundamental cell, two for each layer

Where $\pi = \hbar(k_x + ik_y), \pi^\dagger = \hbar(k_x - ik_y)$, and the velocities $v_{3,4} = a\gamma_{3,4}/\hbar$
are effective fermi velocities that come from the coupling γ_3 and γ_4 CON-
TROLLA SE LA CONVERSIONE DELLA A è CORRETTA
A simple analytic solution may be obtained by neglecting the terms $v_4\pi, v_4\pi^\dagger$
proportional to γ_4, and by considering only interlayer asymmetry U in the
on-site energies: $E_{A_1} = E_{B_1} = -U/2$ and $E_{A_2} = E_{B_2} = U/2$. Then, there is
electron-hole symmetry, i.e., energies may be written $E = \pm E\alpha(\boldsymbol{p}), \alpha \in 1, 2$

$$E_\alpha^2(\boldsymbol{p}) = \frac{\gamma_1^2}{2} + \frac{U^2}{4} + p^2\left(v^2 + \frac{v_3^2}{2}\right) + (-1)^\alpha \sqrt{\Gamma}$$

$$\Gamma = \frac{1}{4}\left(\gamma_1^2 - v_3^2 p^2\right)^2 + v^2 p^2 \left(\gamma_1^2 + U^2 + v_3^2 p^2\right) + 2\zeta\gamma_1 v_3 v^2 \cos(3\theta)$$

(1.88)

were θ is the polar angle of the impulse $\boldsymbol{k} = (k_x, k_y) = k(\cos\theta, \sin\theta)$

Chapter 2

Anomalous Hall effect

The anomalous Hall effect refers to the appearance of a large spontaneous Hall current in ferromagnet in response to an electric field alone [11], and it was first discovered by Hall in 1881 [12]. Despite its century long history and importance, the microscopic characterization of the anomalous Hall effect has been a controversial subject. In the past three main mechanisms have been identified:

- Berry curvature induced Hall effect [13]

- Skew scattering [14]

- Side-jump scattering [15]

The Berry curvature induced Hall effect can be regarded as an *intrinsic contribution* to the conductivity, the other two are regarded as *extrinsic contributions*, this is because they are related to some kind of asymmetry to the scattering with impurities. More precisely the skew scattering deals with the asymmetry that arises with spin-orbit coupling between the electrons and the impurity, while the side jump is a sudden shift in of the electron coordinates during scattering [15]. The effects are illustrated in figure 2.1. The total Hall conductivity is the sum of all three contributions

$$\sigma_H = \sigma_H^{\text{in}} + \sigma_H^{\text{sk}} + \sigma_H^{\text{sj}} \tag{2.1}$$

where σ_H^{in} is the intrinsic contribution given from equation 1.56, σ_H^{sk} is the skew scattering term, which is proportional to the relaxation time τ, and σ_H^{sj} is the side-jump term that is independent of τ.

An important question is to identify the dominant contribution to the anomalous Hall effect (AHE). The way to compare theoretically the magnitude of the contribution rely mainly on semiclassical conduction theory [17], and they express the dominance of the Berry induced Hall effect. In addition, a number of experimental results also gave favorable evidence for the dominance of the intrinsic contribution [18]. Because of this we are going to
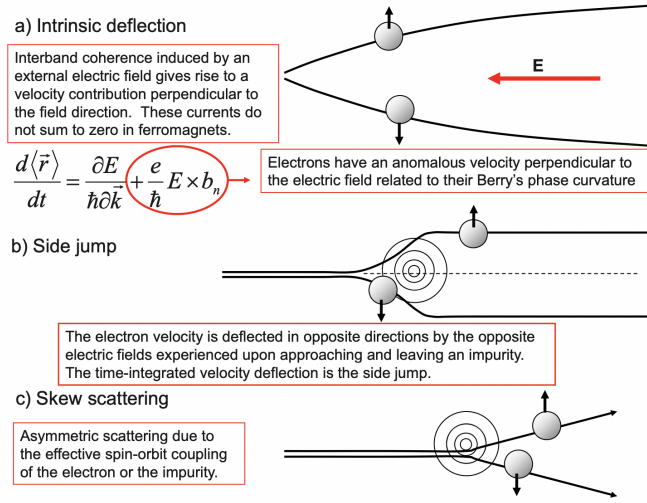
Figure 2.1: All three contributions to the anomalous Hell effect, as you can see the intrinsic contribution does not need an impurity to scatter from. Image taken from [16]

ignore σ_H^{sk} and σ_H^{sj}.

To get used to the math used thought the whole thesis we'll calculate all the anomalous Hall effects exclusively in gapped graphene, however it can be done in several other materials with different hamiltonians.

2.1 Berry curvature in Gapped graphene

The Hamiltonian for the gapped graphene near the point K_1 and K_2 can be written as

$$H_{K_1} = -H_{K_2}^{\dagger} = \begin{bmatrix} \Delta & \hbar v_F(k_x + ik_y) \\ \hbar v_f(k_x - ik_y) & -\Delta \end{bmatrix} \tag{2.2}$$

Where Δ is the energy gap and v_F is the Fermi velocity. For ease of notation we are going to work with just H_{K_1} and drop the K_1,[1] and for ease of computation we define $\boldsymbol{q} = \hbar v_F \boldsymbol{k}$

$$H = \begin{bmatrix} \Delta & q_x + iq_y \\ q_x - iq_y & -\Delta \end{bmatrix} = \sigma_x q_x + \sigma_y q_y + \sigma_z \Delta \equiv \boldsymbol{\sigma} \cdot \boldsymbol{E} \tag{2.3}$$

Here the enegry vector $\boldsymbol{E}$ is defined as $\boldsymbol{E} = (q_x, q_y, \Delta)$. The nice things about it is that $E = |\boldsymbol{E}| = \sqrt{q_x^2 + q_y^2 + \Delta^2}$ is the positive eigenvalue of the

---

[1]Don't worry, I'll bring it back if when we'll need it

hamiltonian (the negative eigenvalue is just $-E$).

To calculate the Berry curvature we are first going to calculate the Berry connection 1.16, and to calultate the Berry connection we need the eigenvectors which are well known for the Hamiltonian of the form $\boldsymbol{\sigma} \cdot \boldsymbol{E}$.

$$|+;\theta,\phi\rangle = \begin{bmatrix} \cos\frac{\theta}{2} \\ e^{i\phi}\sin\frac{\theta}{2} \end{bmatrix} \quad |-;\theta,\phi\rangle = \begin{bmatrix} -e^{-i\phi}\sin\frac{\theta}{2} \\ \cos\frac{\theta}{2} \end{bmatrix} \tag{2.4}$$

Where θ and ϕ are the coordinates of $\boldsymbol{E}$ in the polar representation

Now we can calculate the Berry connection

$$A_\theta^+ = -A_\theta^- = 0 \quad A_\phi^+ = -A_\phi^- = \sin^2\frac{\theta}{2} \tag{2.5}$$

This means that the Berry curvature is

$$\Omega_{\theta\phi}^+ = -\Omega_{\theta\phi}^- = \partial_\theta A_\phi^+ = \frac{\sin\theta}{2} \tag{2.6}$$

From now on we are going to work with Ω^+ and we are going to drop the $+$ sign to make the notation lighter.

We want to express Ω in terms of $\boldsymbol{q}$, however it's more convenient to write it in terms fo $\cos\theta$ and ϕ, so we do a small coordinate transformation

$$\Omega_{\theta\phi} = \frac{\partial\cos\theta}{\partial\theta}\Omega_{\cos(\theta)\phi} \rightarrow \Omega_{\cos(\theta)\phi} = \frac{1}{2} \tag{2.7}$$

Now we can easily make the transformation to express Ω in terms of $\boldsymbol{q}$. The Berry curvature transforms like any other tensor under coordinate transformation, so

$$\Omega_{q_x q_y} = \frac{\partial\cos\theta}{\partial q_x}\frac{\partial\phi}{\partial q_y}\Omega_{\cos(\theta)\phi} + \frac{\partial\phi}{\partial q_x}\frac{\partial\cos\theta}{\partial q_y}\Omega_{\phi\cos(\theta)} \tag{2.8}$$

That can be rewritten as

$$\Omega_{q_x q_y} = \frac{1}{2}\det\left[\frac{\partial(cos\theta,\phi)}{\partial(q_x,q_y)}\right] = \frac{1}{2}\frac{\Delta^2}{q^2 E^3}(q_x + q_y - 2q) \tag{2.9}$$

And finally we can express it in terms of $\boldsymbol{k}$

$$\Omega_{k_x k_y} = (\hbar v_F)^2\Omega_{q_x q_y} = \frac{\hbar v_F}{2}\frac{\Delta^2}{k^2 E^3}(k_x + k_y - 2k) \tag{2.10}$$

Up until now we have worked with the Hamiltonian H_{K_1}, but with the K_1 hidden. The Berry curvature around K_2 is equal, but with opposite sign (figure 2.2) [2]

---

[2]A short proof for it can be the following: If we send $k_y \rightarrow -k_y$ we effectively send $H_{K_1} \rightarrow H_{K_2}$.
The berry curvature can be written as $\Omega_{k_x k_y} = i\langle\partial_{k_x}n| \wedge |\partial_{k_y}n\rangle$. By sending $k_y \rightarrow -k_y$ we have that $\Omega \rightarrow -\Omega$.
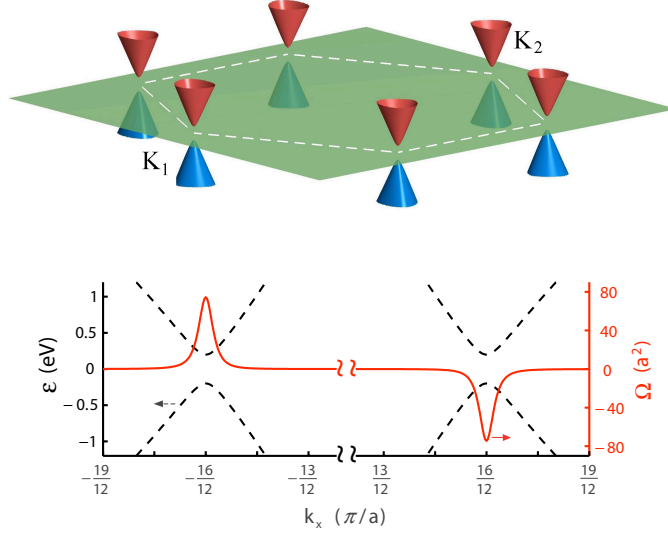
Figure 2.2: In the top panel are displayed the Energy bands in 2D. In the bottom panel with the dotted line are displayed a section of the energy bands, and with the continuous red line the Berry curvature.

2.2 Spin Hall effect

The most famous example of anomalous Hall effect is the spin Hall effect (SHE). It is a phenomenon arising due to spin-orbit coupling in which change current passing thought a sample leads to spin transport in the transverse direction [19]. This phenomenon has been attracting continuous interest, and it is one of the protagonists of the field of spintronics [20].

Due to relativistic corrections, an electron moving with velocity $\boldsymbol{v}$ in an electric field $\boldsymbol{E}$ will experience a magnetic field

$$\boldsymbol{B} = -\frac{1}{c}(\boldsymbol{v} \times \boldsymbol{E}) \tag{2.11}$$

This means that the spin-orbit coupling term of the Hamiltonian is

$$H_{\mathrm{SO}} = -\frac{g\mu_B}{2}\boldsymbol{B} \cdot \boldsymbol{s} = \alpha_R(\boldsymbol{k} \times \boldsymbol{E}) \cdot \boldsymbol{s} \tag{2.12}$$

where $-g\mu_B/2$ is the electron magnetic moment, and $\alpha_R = g\mu_B/2\hbar mc$. We can assume that the electric field is equal to $\boldsymbol{E} = E_z\hat{\boldsymbol{z}}$, this is achieved either by a perpendicular electric field or by interaction with a substrate. With this we get the Rashba spin-orbit interaction also called as the external spin-orbit interaction[21]

$$H_{\mathrm{SO}}^{\mathrm{ext}} = \alpha_R E_z(\boldsymbol{s} \times \boldsymbol{k}) \cdot \hat{\boldsymbol{z}} \tag{2.13}$$

33

It can be show that this is equal to [22] QUA VOLENDO POSSO MET-TERCI I PASSAGGI

$$H_{\text{SO}}^{\text{ext}} = \lambda_R(\sigma_x \tau_z s_y - \sigma_y s_x) \tag{2.14}$$

Where in the last equation the same notation from equation 1.81. Another contribution due to the spin-orbit interaction comes from the interaction with the honeycomb periodic potential. If we plug $\boldsymbol{E} = \nabla V$ into equation 2.12 we get

$$H_{\text{SO}}^{\text{int}} = \alpha_R(\boldsymbol{k} \times \nabla V) \cdot \boldsymbol{s} \tag{2.15}$$

Kane and Mele [22] showed that this is equivalent to

$$H_{\text{SO}}^{\text{int}} = \Delta_{\text{SO}}\, \sigma_z \tau_z s_z \tag{2.16}$$

2.3 Valley-Hall effect

The Hall conductivity σ_{xy} is

$$\sigma_{xy} = \frac{e^2}{\hbar} \int_{\mathbb{R}^2} f[E^+(k)]\Omega_{k_x k_y}^+ + f[E^-(k)]\Omega_{k_x k_y}^- \frac{d^2 \boldsymbol{k}}{2\pi} \tag{2.17}$$

Where $f(E) = \left[e^{\beta(E-\mu)} + 1\right]^{-1}$ is the Fermi-Dirac distribution, it is applied once for the states with positive energy and once for the states with negative energy.

We are going to analyze the system at low temperatures ($k_\beta T \ll 1$), so our Fermi-Dirac distribution can be considered like a step-function.

First let's integrate the conductivity for the positive energies and drop the $+$ sign to make the notation lighter.

$$\int_{\mathbb{R}^2} f[E(k)]\Omega_{k_x k_y} dk_x dk_y = \int_{\mathbb{R}^2} f[E(q)]\Omega_{q_x q_y} dq_x dq_y \approx$$

$$\approx \int_0^{2\pi} \int_0^{q_F} \frac{1}{2} \frac{\Delta^2}{q^2 E^3}(q_x + q_y - 2q) q\, dq\, d\theta =$$

$$= -2\pi\Delta^2 \int_0^{q_f} \frac{dq}{E^2} = -2\pi\Delta^2 \int_0^{q_f} \frac{dq}{(\Delta^2 + q^2)^{3/2}} = -\frac{2\pi q_F}{\sqrt{\Delta^2 + q_F^2}}$$

And now we express it in terms of the chemical potential μ [3]

$$\int_{\mathbb{R}^2} f[E(k)]\Omega_{k_x k_y} dk_x dk_y \approx -2\pi \frac{\sqrt{\mu^2 - \Delta^2}}{\mu}\theta(\mu - \Delta) \tag{2.18}$$

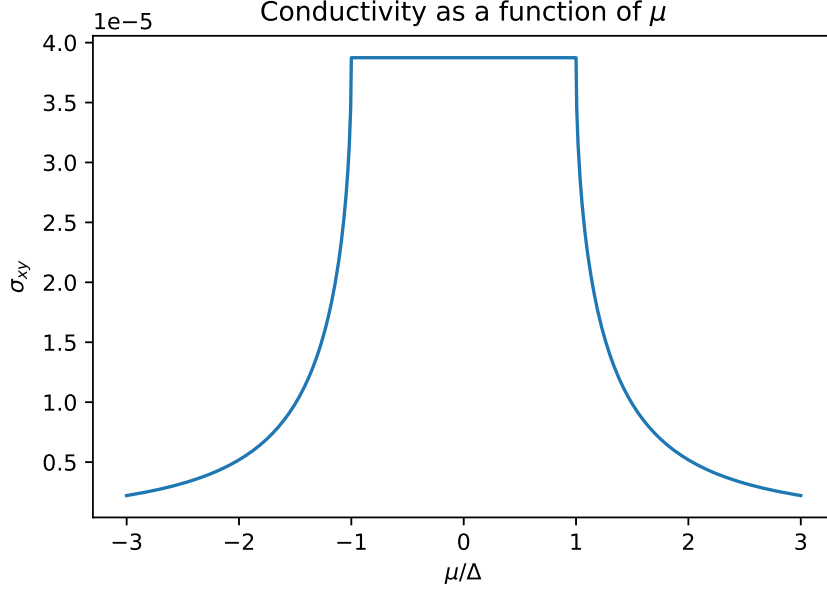[3]Here we can use interchangeably μ and E_F

Figure 2.3: Here is shown $\sigma_{xy}(\mu)$ (eq. 2.19). Notice how, when $\mu \in [-\Delta, \Delta]$ then $\sigma_{xy} = \frac{e^2}{2\pi\hbar}$

The $\theta(\mu - \Delta)$ is there to make sure that if no states are inside the Fermi-Dirac the integral is zero. One thing to notice is that if you have $\mu \gg \Delta$ (aka. all states in the band are occupied) then the integral is equal to -2π. The integral of the lower band is very similar. By the end equation of the conductivity 2.17 becomes

$$\sigma_{xy}(\mu) = -\frac{e^2}{2\pi\hbar}\left[\frac{\sqrt{\mu^2 - \Delta^2}}{\mu}\theta(\mu^2 - \Delta^2) - \theta(\mu - \Delta)\right] \qquad (2.19)$$

To be fear we only calculated σ_{xy} for the electrons in the valley K_1, the conductivity for the other valley is just $-\sigma_{xy}$. So, putting it all together, we have

$$\sigma_{K_i,xy}(\mu) = (-1)^i\frac{e^2}{2\pi\hbar}\left[\frac{\sqrt{\mu^2 - \Delta^2}}{\mu}\theta(\mu^2 - \Delta^2) - \theta(\mu - \Delta)\right] \qquad (2.20)$$

However in most cases it's safe to assume that the chemical potential is inside the energy gap, so equation 2.20 becomes

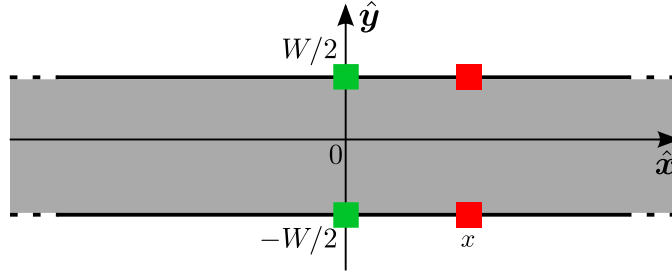$$\sigma_{K_i,xy} = (-1)^{i+1}\frac{e^2}{2\pi\hbar} \qquad (2.21)$$

Figure 2.4: Representation of the strip

2.4 Non-local Charge transport

If we apply a voltage V in two opposite points of a strip of a ohmic material of width W and infinite lenght, and we see a current that flows from one point to another figure 2.4.

Clearly the current isn't completely localized along the axis that unites the two injection points, and so does the voltage difference.

If we probe the voltage from two different points with an offset of x from the injection points and we divide it by the total current between the contacts we see that

$$\frac{V(x)}{I} = \frac{2\rho}{\pi} \ln \left| \coth \left(\frac{\pi x}{2W} \right) \right| \tag{2.22}$$

Where ρ is the resistivity. Don't worry later on there is the proof of this equation.

However, two-dimentional material like gapped graphene [23–25] and transition metal dichalcogenides [26–28], don't obey this equation. This is because theese materials display the Valley Hall effect we talked about previously (inserire reference a sezione).

Non-local transport can be a useful tool to probe the existance of anomalous Hall effect [29–34]

2.5 Theory of non local charge transport

The charges inside the material get pushed around from the electrochemical potential ψ_K

$$\psi_K(\boldsymbol{r}) = V(\boldsymbol{r}) - \frac{1}{e} \mu_K[n_{K_1}(\boldsymbol{r}), n_{K_2}(\boldsymbol{r}), T] \tag{2.23}$$

Where ϕ is the electrical potential, and $\mu_K = \frac{\partial}{\partial n_K} F[n_{K_1}(\boldsymbol{r}), n_{K_2}(\boldsymbol{r}), T]$ is the chemical potential of the material and F is the free energy.

The current generated from this potential in the valley K_α in the $i-$th direction is

$$-eJ_{K_\alpha,i}(\boldsymbol{r}) = \sum_{j,b} \underbrace{-\sigma_{K_\alpha K_\beta,ij}}_{\text{conductivity}} \partial_j \psi_{K_\beta}(\boldsymbol{r}) \qquad (2.24)$$

From now we are going to set $T \approx 0^4$ and ignore intervalley scattering, so if $K_\alpha \neq K_\beta$ $\sigma_{K_\alpha K_\beta,ij} = 0$, also because of this the free energy can be written as the sum of the two Free energies

$$F(n_{K_1}, n_{K_2}) = F_1(n_{K_1}(\mathbf{r})) + F_2(n_{K_2}(\mathbf{r})) \qquad (2.25)$$

And so the chemical potential of a given valley depend only on the number of electron in the same valley

$$\mu_\alpha(n_{K_\alpha}(\mathbf{r})) = \frac{\partial}{\partial n_{K_\alpha}} F(n_{K_0}, n_{K_1}) = \frac{\partial}{\partial n_{K_\alpha}} F_\alpha(n_{K_\alpha}(\mathbf{r})) \qquad (2.26)$$

This simplifies the trasport equation in

$$-e\mathbf{J}_{K_\alpha}(\mathbf{r}) = \sigma_{K_\alpha}(\mathbf{r})\nabla\psi_{K_\alpha}(\mathbf{r}) \qquad (2.27)$$

Where σ_{K_α} is the following matrix

$$\sigma_{K_\alpha} = \begin{bmatrix} \sigma_{K_\alpha K_\alpha,xx} & \sigma_{K_\alpha K_\alpha,xy} \\ -\sigma^*_{K_\alpha K_\alpha,xy} & \sigma_{K_\alpha K_\alpha,xx} \end{bmatrix}$$

Now we need to write the gradient electrochemical potential $\nabla\psi(\boldsymbol{r})$

$$\nabla\psi_{K_\alpha}(\mathbf{r}) = \nabla V(\mathbf{r}) - \frac{1}{e}\frac{\partial}{\partial n_{K_\alpha}}\mu_\alpha(n_{K_\alpha}(\mathbf{r}))\nabla n_{K_\alpha} \qquad (2.28)$$

From equation INSERIRE REFERENCE A EQUAZIONE we can write for gapped Dirac hamiltonians that VERIFICARE SE VALE ANCHE PER BILAYER GRAPHENE

$$\frac{\partial \mu_{K_\alpha}}{\partial n_{K_\alpha}} = \frac{\pi}{\sqrt{2\pi|n| + \Delta^2}} + \Delta\delta(n) \approx \frac{\pi}{\Delta} + \Delta\delta(n) \quad \forall \alpha$$

In this equation we assumed that there are very few charge carries, so $\frac{n}{\Delta^2} \approx 0$. We can shorten the equation 2.28 by defining

$$e^2 D_{K_\alpha,ij} = \sigma_{K_\alpha,ij}\frac{\partial \mu_\alpha}{\partial n_{K_\alpha}}[n_{K_\alpha}(\mathbf{r})] \qquad (2.29)$$

---

[4]A more precise statement is that the thermal De Broglie wavelenght λ_T must be much larger than the average distance between the electrons. We are not going into the math here, but if you want to calculate it, keep in mind that the dispersion relation is relativistic, so the formula of λ_T is going to be a bit different

So equation 2.27 becomes

$$-eJ_{K_\alpha,i}(\mathbf{r}) = \sigma_{K_\alpha,ij}E_j(\mathbf{r}) - eD_{K_\alpha,ij}\partial_j n_{K_\alpha}(\mathbf{r}) \qquad (2.30)$$

or, written in matrix form

$$-e\mathbf{J}_{K_\alpha}(\mathbf{r}) = \sigma_{K_\alpha}\mathbf{E}(\mathbf{r}) - eD_{K_\alpha}\nabla n_{K_\alpha}(\mathbf{r}) \qquad (2.31)$$

Where σ_{K_α} and $-eD_{K_\alpha}$ are matrices.

2.5.1 Re-writing the equations in terms of charge current and valley current

Measuring the currents in different valley can be cumbersome, however measuring the charge current $\mathbf{J}_c = \mathbf{J}_{K_1} + \mathbf{J}_{K_2}$ is straightforward, and for mathematical convenience we also define the valley current $\mathbf{J}_v = \mathbf{J}_{K_1} - \mathbf{J}_{K_2}$.

Since we no longer describe the currents in terms of their valley index, but on the sum and the difference of what happens at the different valleys, we are going to reparametrize also the other quantities in the same fashion.

$$\begin{cases} \sigma_c = \sigma_{K_1} + \sigma_{K_2} = 2\sigma_{xx}\delta_{ij} \\ \sigma_v = \sigma_{K_1} - \sigma_{K_2} = \sigma_v = 2\sigma_{xy}\epsilon_{ij} \end{cases} \qquad (2.32)$$

The term $-eD_{K_\alpha}\nabla n_{K_\alpha}(\mathbf{r})$ is a little harder to traslate. First off we are going to impose the local charge conservation

$$n(\mathbf{r}) = n_{K_0} + n_{K_1} \approx 0$$

and so

$$n_v(\mathbf{r}) = n_{K_1} - n_{K_2} = 2n_{K_1} = -2n_{K_2} \qquad (2.33)$$

Now let's do the sum of the $D_{K_\alpha}\nabla n_{K_\alpha}(\mathbf{r})$ terms to write them in terms of charge and valleys degrees of freedom

$$D_{K_1}\nabla n_{K_1} + D_{K_2}\nabla n_{K_2} = (D_{K_1} - D_{K_2})\nabla n_v(\mathbf{r})/2$$

$$D_{K_1} - D_{K_2} = \sigma\frac{\partial\mu_1}{\partial n_{K_1}} - \sigma^T\frac{\partial\mu_2}{\partial n_{K_2}}$$

since $\mu_v = 2\mu_1 = -2\mu_2$ and $n_v = 2n_{K_1} = -2n_{K_2}$

$$D_{K_1} - D_{K_2} = \frac{1}{e^2}(\sigma - \sigma^T)\frac{\partial\mu_v}{\partial n_v} = \frac{2}{e^2}\sigma_v\frac{\partial\mu_v}{\partial n_v}$$

so I define

$$D_{cv} = \frac{2}{e^2}\sigma_v\frac{\partial\mu_v}{\partial n_v} \approx \frac{2}{e^2}\frac{\pi}{\Delta}\sigma_v$$

so we get that

$$D_{K_1}\nabla n_{K_1} + D_{K_2}\nabla n_{K_2} = D_{cv}n_v$$

Putting it all together we have that

$$\mathbf{J}_c(\mathbf{r}) = \sigma_c\mathbf{E}(\mathbf{r}) + eD_{cv}\nabla n_v(\mathbf{r})$$

Writing all the indices

$$J_{c,i} = \sum_j \sigma_{c,xx}\delta_{ij}E_i + D_{cv,xy}\epsilon_{ij}\partial_j n_v \tag{2.34}$$

so we can rewrite them as

$$\mathbf{J}_c = \sigma_{c,xx}\mathbf{E}_i + D_{cv,xy}\nabla \times n_v \tag{2.35}$$

where $\sigma_{c,xx}$ and $D_{cv,xy}$ are scalars.

And now the difference of the $D_{K_\alpha}\nabla n_{K_\alpha}(\mathbf{r})$ terms to write them in terms of charge and valleys degrees of freedom

$$D_{K_0}\nabla n_{K_0} - D_{K_1}\nabla n_{K_1} = (D_{K_0} + D_{K_1})\nabla n_v(\mathbf{r})/2$$

and with some calculations done in a similar fashion to the one we use to calculate $\mathbf{J}_c$ we have that

$$D_v = \frac{1}{2}(D_{K_0} + D_{K_1}) = \frac{1}{e^2}\sigma_c\frac{\partial \mu_c}{\partial n_c}$$

so, in matrix form

$$\mathbf{J}_v(\mathbf{r}) = \sigma_v\mathbf{E}(\mathbf{r}) + eD_v\nabla n_v(\mathbf{r}) \tag{2.36}$$

which can be re-written as

$$J_{v,i}(\mathbf{r}) = \sum_j \sigma_{c,xy}\epsilon_{ij}E_j(\mathbf{r}) + eD_{v,xx}\delta_{ij}\partial_j n_v(\mathbf{r}) \tag{2.37}$$

where $\sigma_{c,xy}$ and $D_{v,xx}$ are scalars

2.5.2   Laplace equation

Now that we have the charge and valley currents differential equations we calculate the laplacians to solve them. Let's start from the equation for the charge currents 2.35

$$\nabla \cdot \boldsymbol{J}_c = \nabla \cdot (\sigma_c\mathbf{E}) + eD_{cv,xx}\nabla \cdot (\nabla \times n_v) \tag{2.38}$$

Inside the material the are no sources of charge current, so $\nabla \cdot \boldsymbol{J}_c =$, and the divergence of a rotor is zero, so $\nabla \cdot (\nabla \times n_v) = 0$. This means that inside the material

$$\boxed{\nabla^2 V(x,y) = 0} \tag{2.39}$$

So, to be able to solve the laplace equation we just need to impose the boundary conditions that the current is injected in a single point at $x = 0$ along the $\hat{\boldsymbol{y}}$ direction.

$$-e\boldsymbol{J}_c(x, \pm W/2) = I\delta(x)\hat{\boldsymbol{y}}$$

If we put it in equation 2.38 we get

$$\boxed{I\delta(x) = \sigma_{c,xx}\partial_y V(x, \pm W/2) - eD_{cv,xy}\partial_x n_v(x, \pm W/2)} \tag{2.40}$$

Now let's calculate the laplacian for the valley current equation 2.37

$$\nabla \cdot \mathbf{J}_v = \nabla \times (\sigma_{c,xy}\mathbf{E}) + e\nabla \cdot (D_{v,xx}\nabla n_v) \tag{2.41}$$

Now, lets analyze all the terms one by one

- For the continuity equation we have that $\nabla \cdot \mathbf{J}_v = \frac{\partial}{\partial t}n_v$, since intervalley scattering is zero, this should be zero, but why don't add it back now? so we say that it decays exponentially $\frac{\partial}{\partial t}n_v = -\frac{1}{\tau_v}n_v$

- $e\nabla \cdot (D_{v,xx}\nabla n_v)$ is really nothing special, inside the material $D_{v,xx}$ is constsant so in the end it is equal to $eD_{v,xx}\nabla^2 n_v$

- $\nabla \times (\sigma_{c,xy}\mathbf{E})$ is equal to zero inside the material, but on the edge can be non-zero because $\sigma_{c,xy}$ changes form inside to the outside

In the end we get that

$$eD_{v,xx}\nabla^2 n_v = -\frac{1}{\tau_v}n_v - \nabla \times (\sigma_{c,xy}\mathbf{E}) \tag{2.42}$$

This means that at the equilibrium $n_v \neq 0$ only if you are were $\nabla \times (\sigma_{c,xy}\mathbf{E}) \neq 0$, and this is only true along the edge, so we we'll have to worry about this term only in the boundary conditions, So

$$\boxed{\left[\nabla^2 - \frac{1}{\tau_v D_{v,xx}}\right]n_v(\boldsymbol{r}) = 0} \tag{2.43}$$

The boundary condition is simply that the valley current doesn't exit the material, so

$$J_{v,y}(x, \pm W/2) = 0 \tag{2.44}$$

putting it into the differential equation for J_v (eq 2.37) we get

$$\boxed{\sigma_{v,xy}\partial_x V(x, \pm W/2) + eD_{v,xx}\partial_y n_v(x, \pm W/2) = 0} \tag{2.45}$$

All the boxed equations we wrote in the in this section enable us to completely solve the system. For convenience let's write the m in a single system of equations

$$
\begin{cases}
\nabla^2 V(x,y) = 0 \\
\left[\nabla^2 - \frac{1}{\tau_v D_{v,xx}}\right] n_v(\boldsymbol{r}) = 0 \\
I\delta(x) = \sigma_{c,xx}\partial_y V(x,\pm W/2) - eD_{cv,xy}\partial_x n_v(x,\pm W/2) \\
\sigma_{v,xy}\partial_x V(x,\pm W/2) + eD_{v,xx}\partial_y n_v(x,\pm W/2) = 0
\end{cases}
\tag{2.46}
$$

From the third equation in the system above we can see that $V(x,y)$ is even along the $\hat{\boldsymbol{x}}$ axis and odd along the $\hat{\boldsymbol{y}}$ axis.

From the fourth equation we can see that n_v has the opposite parity to V, so it's odd along the $\hat{\boldsymbol{x}}$ axis and even along the $\hat{\boldsymbol{y}}$ axis.

To be able to solve it we first have to do a fourier transform over the $\hat{\boldsymbol{x}}$ direction. The first two equations of eq 2.46 become

$$
\begin{cases}
(\partial_y^2 - k^2)V(k,y) = 0 \\
\left[\partial_y^2 - \omega^2(k)\right]n_v(k,y) = 0
\end{cases}
\tag{2.47}
$$

And the solutions that respect the symmetries we talked about earlier are

$$
V(k,y) = V(k)\sinh(ky) \qquad n_v(k,y) = n_v(k)\cosh[\omega(k)y]
\tag{2.48}
$$

However we still don't know what are $V(k)$ and $n_v(k)$, to obtain them we have to plug the equations above in the last two equations of 2.46

$$
\begin{cases}
\sigma_{c,xx}k\cosh(kw/2)V(k) - eD_{cv,xy}ik\cosh(\omega W/2)n_v(k) = I \\
-\sigma_{v,xy}ik\sinh(kw/2)V(k) - eD_{v,xx}\omega(k)\sinh(\omega W/2)n_v(k) = 0
\end{cases}
\tag{2.49}
$$

This system of equation is linear in $V(k)$ and $n_v(k)$, so it can be written in this form

$$
\begin{bmatrix} A & B \\ C & D \end{bmatrix} \begin{bmatrix} V \\ n_v \end{bmatrix} = \begin{bmatrix} I \\ 0 \end{bmatrix}
\tag{2.50}
$$

And the inverse is simply

$$
\begin{bmatrix} V \\ n_v \end{bmatrix} = \frac{I}{AD - BC} \begin{bmatrix} D \\ -C \end{bmatrix}
\tag{2.51}
$$

Since we want only care to calculate the voltage we only need to evaluate

$$
V = \frac{I}{A - \frac{BC}{D}}
$$

wich turns out to be equal to

$$V(k) = \frac{I}{\sigma_c} \frac{\omega(k)/k}{\sinh(kW/2)} \left\{ \frac{\omega(k)}{\tanh(kW/2)} + \frac{k\tan^2(\theta_{VH})}{\tanh[\omega(k)W/2]} \right\}^{-1} \qquad (2.52)$$

We can plug it into equation 2.48 and evaluate it at $y = \pm W/2$

$$V(k, \pm W/2) = V(k)\sinh(\pm kW/2) = \frac{I\omega}{\sigma_c k} \left\{ \dots \right\}^{-1} \qquad (2.53)$$

Where the terms inside the curly brakets are the same from the previous equation (2.52).

Finally we can calculate the non-local resistance

$$R_{NL}(k) = \frac{V(k, W/2) - V(k, -W/2)}{I} \qquad (2.54)$$

Which is equal to

$$R_{NL}(k) = \frac{2\omega(k)}{k\sigma_c} \left\{ \frac{\omega(k)}{\tanh(kW/2)} + \frac{k\tan^2(\theta_{VH})}{\tanh[\omega(k)W/2]} \right\}^{-1} \qquad (2.55)$$

Chapter 3

Theory of the non-local resistance

Let's from the frequency response of the non-local response that we talked about in section **??** [35]

$$R_{\mathrm{NL}}(k) = \frac{2\omega(k)}{k\sigma_c}\left\{\frac{\omega(k)}{\tanh(kW/2)} + \frac{k\tan^2(\theta_{\mathrm{VH}})}{\tanh[\omega(k)W/2]}\right\}^{-1} \tag{3.1}$$

Its anti-fourier transform tells us everything we would want to know about the system. Unfortunately 3.1 doesn't have an analytic Fourier transform. If there are no topological effect $\theta_{\mathrm{VH}} = 0$ and it can be solved analytically.

$$R_{\mathrm{NL}}(k)|_{\theta_{\mathrm{VH}}=0} \equiv R_{\mathrm{NL}}^{(0)}(k) = \frac{2\rho}{k}\tanh\left(\frac{kW}{2}\right) \tag{3.2}$$

$$R_{\mathrm{NL}}^{(0)}(x) = \mathcal{F}^{-1}\left[R_{\mathrm{NL}}^{(0)}(k)\right] = -\frac{2\rho}{\pi}\ln\left|\tanh\left(\frac{\pi x}{2W}\right)\right| \tag{3.3}$$

This is the purely ohmic nonlocal signal that we have talked about in 2.22. However, if we are going to explore topological materials we cannot set $\tan(\theta_{\mathrm{VH}}) = 0$, this means that we'll have to do some approximations.

3.1 Study of $R_{\mathrm{NL}}(x)$

Let's look at the graph of the $R_{\mathrm{NL}}(k)$ before doing any approximations: As you can see from the figure 3.1

- If $W \gg l_{\mathrm{v}}$ we have a single bell like function with the width of the bell being $\approx 1/W$ and the height being R_{xx}

- If $W \ll l_{\mathrm{v}}$ we have a double-bell function, where the first bell has a height of R_{xx} and a width of $\approx 1/l_{\mathrm{v}}$, and the second one has a shorter height.
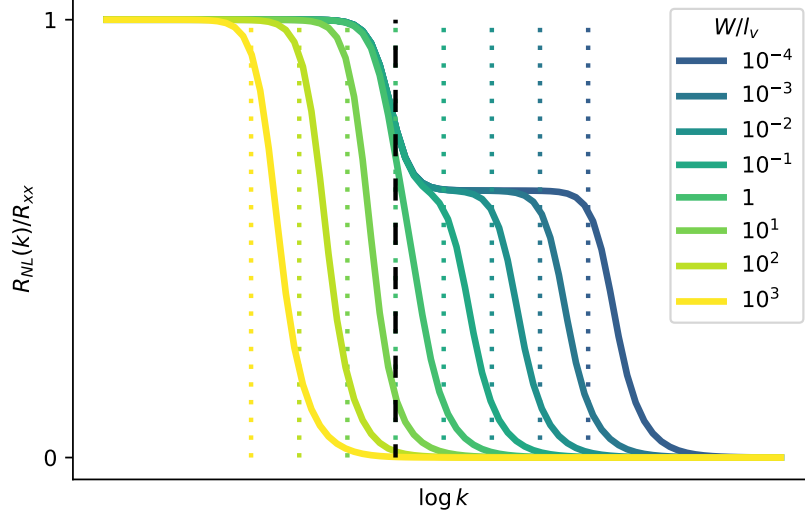
Figure 3.1: $R_{NK}(k)$ for several values of W/l_{v}. The dashed black line represents where $k = 1/l_{\mathrm{v}}$, the colored dashed line represents where $k = 1/W$

To evaluate the precise height of the secondary bell we just need to set $l_{\mathrm{v}}^{-1} \ll k \ll W^{-1}$ in equation 3.1, this gives us

$$R_{\mathrm{NL}}(l_{\mathrm{v}}^{-1} \ll k \ll W^{-1}) \approx R_{xx} \cos^2(\theta_{\mathrm{VH}}) \tag{3.4}$$

Where $R_{xx} = \frac{W}{\sigma_{xx}}$ and $\cos^2(\theta_{\mathrm{VH}}) = \frac{1}{1+\tan^2(\theta_{\mathrm{VH}})}$

So, if we have $l_{\mathrm{v}} \ll W$ or $\theta_{\mathrm{VH}} \ll 1$ (or both) we have a single bell structure. Incidentally these are the conditions to NOT have topological effects, so the less visible the double bell is, the less visible the topological effects are. We'll also see later how one of the bell represents the ohmic nonlocal signal, while the other represents the topological nonlocal signal.

3.1.1 Small k

Let's start by exploring $k \ll l_{\mathrm{v}}^{-1}, W^{-1}$. This will tell us how the function behaves at long ranges $x \gg l_{\mathrm{v}}, W$. In this regime

$$\omega(k) = \sqrt{k^2 + l_{\mathrm{v}}^{-2}} \approx \frac{1}{l_{\mathrm{v}}}\left[1 + \frac{(kl_{\mathrm{v}})^2}{2}\right] \tag{3.5}$$

$$\coth(kW/2) \approx \frac{2}{kW} + \frac{kW}{6} \tag{3.6}$$

Plugging the last two equations into equation 3.1 we have that $R_{\mathrm{NL}}(k) \approx$

$$\frac{2}{\sigma_c}\frac{1}{l_{\mathrm{v}}k}\left[\frac{1}{l_{\mathrm{v}}}\left(1+\frac{k^2 l_{\mathrm{v}}^2}{2}\right)\left(\frac{2}{kW}+\frac{kW}{6}\right)+\frac{k\tan^2(\theta_{\mathrm{VH}})}{\tanh(W/2l_{\mathrm{v}})}+o(k^2)\right]^{-1} \quad (3.7)$$

And after some steps we get that

$$R_{\mathrm{NL}}(k \ll l_{\mathrm{v}}^{-1}, W^{-1}) = \frac{R_{xx}}{1+L_{\mathrm{v}}^2 k^2 + o(k^4)} \quad (3.8)$$

Where the *renormalized valley diffusion length* L_{v}^2 is defined as

$$L_{\mathrm{v}}^2 \equiv l_{\mathrm{v}}^2 + \frac{W^2}{12} + \frac{l_{\mathrm{v}}W}{2}\frac{\tan^2(\theta_{\mathrm{VH}})}{\tanh(W/2l_{\mathrm{v}})} \quad (3.9)$$

Now we are going to define the topological nonlocal resistance R_{NL}^T by taking the equation 3.8, and ignoring the $o(k^4)$ term

$$R_{\mathrm{NL}}^T(k) \equiv \frac{R_{xx}}{1+L_{\mathrm{v}}^2 k^2} \quad (3.10)$$

We are now ready to do the Fourier transform of equation 3.10 to get the behavior for $x \gg l_{\mathrm{v}}, W$

$$R_{\mathrm{NL}}(x \gg l_{\mathrm{v}}, W) \approx \mathcal{F}^{-1}\left[R_{\mathrm{NL}}^T(k)\right] \equiv R_{\mathrm{NL}}^T(x) \quad (3.11)$$

That is equal to

$$R_{\mathrm{NL}}^T(x) = R_{xx}\int_{-\infty}^{+\infty}\frac{e^{-ikx}}{1+L_{\mathrm{v}}^2 k^2}\frac{dk}{2\pi} = \frac{R_{xx}}{2L_{\mathrm{v}}}e^{-\frac{|x|}{L_{\mathrm{v}}}} \quad (3.12)$$

So,

$$R_{\mathrm{NL}}(x \gg l_{\mathrm{v}}, W) \approx R_{\mathrm{NL}}^T(x) \quad (3.13)$$

3.1.2   Big k

Fortunately the case for which $k \gg l_{\mathrm{v}}^{-1}$ is much simpler: in this case $\omega(k) \approx k$, so

$$R_{\mathrm{NL}}(k \gg l_{\mathrm{v}}^{-1}) = \cos^2(\theta_{\mathrm{VH}})\frac{2\rho}{k}\tanh\left(\frac{kW}{2}\right) \quad (3.14)$$

Using equation 3.2 we get that this last equation is $\cos^2(\theta_{\mathrm{VH}})$ times the one for the purely ohmic nonlocal signal

$$R_{\mathrm{NL}}(k \gg l_{\mathrm{v}}^{-1}) \approx \cos^2(\theta_{\mathrm{VH}})R_{\mathrm{NL}}^{(0)}(k) \quad (3.15)$$

This means that the Fourier transform is

$$R_{\mathrm{NL}}(x \ll l_{\mathrm{v}}) \approx \cos^2(\theta_{\mathrm{VH}})R_{\mathrm{NL}}^{(0)}(x) \quad (3.16)$$
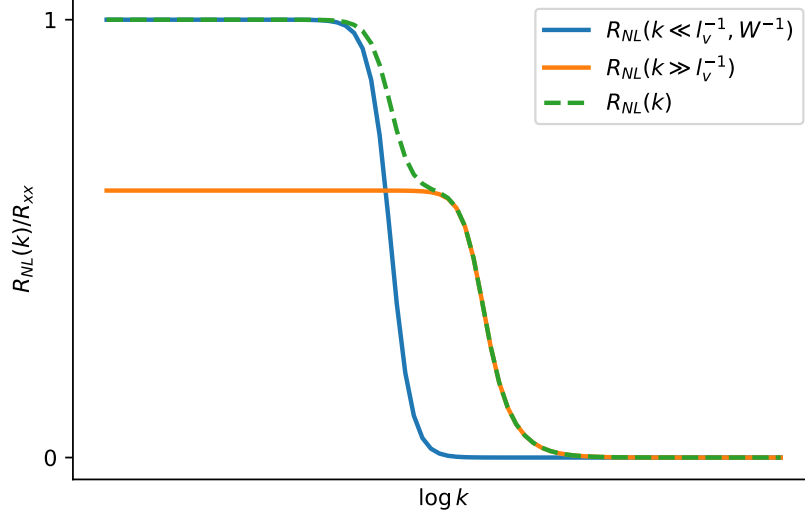
Figure 3.2: For this example $l_\mathrm{v} = 20W$

3.1.3 Testing the approximations

But how do these equations fear in practice? As you can see from figure 3.2 the two approximations work pretty well, except in the neighborhood where $k \approx l_\mathrm{v}^{-1}$. But what we really care about is $R_\mathrm{NL}(x)$.

If we plot the approximations for $x \gg l_\mathrm{v}, W$ (eq. 3.13) and $x \ll l_\mathrm{v}$ (eq. 3.16) alongside the numerical Fourier transform of $R_\mathrm{NL}(k)$ 3.1 we get figure 3.3

3.1.4 Improving the approximation

We can do better than this! By combining the two approximations it's possible to have a single equation that is very accurate for both $x \gg l_\mathrm{v}, W$ and $x \ll l_\mathrm{v}$, however, in the end we'll end up with an approximation that is surprisingly good even for $x \approx l_\mathrm{v}$.

Since the Fourier transform is a linear operator, the idea is to find the linear combination of the two approximation that best approximates the $R_\mathrm{NL}(k)$ for both $k \ll l_\mathrm{v}^{-1}, W^{-1}$ and $k \gg l_\mathrm{v}^{-1}$ and then anti-transform the result.

$$R_\mathrm{NL}(k) \approx \alpha R_\mathrm{NL}(k \ll l_\mathrm{v}^{-1}, W^{-1}) + \beta R_\mathrm{NL}(k \gg l_\mathrm{v}^{-1}) =$$

$$= R_\mathrm{NL}(k) \approx \alpha R_\mathrm{NL}^{T}(k) + \beta \cos^2(\theta_\mathrm{VH}) R_\mathrm{NL}^{(0)}(k)$$

Where α and β are the coefficient to be determined.

Since we only need to evaluate two variables, we only need to evaluate the expression above in two different points. The most reasonable points to
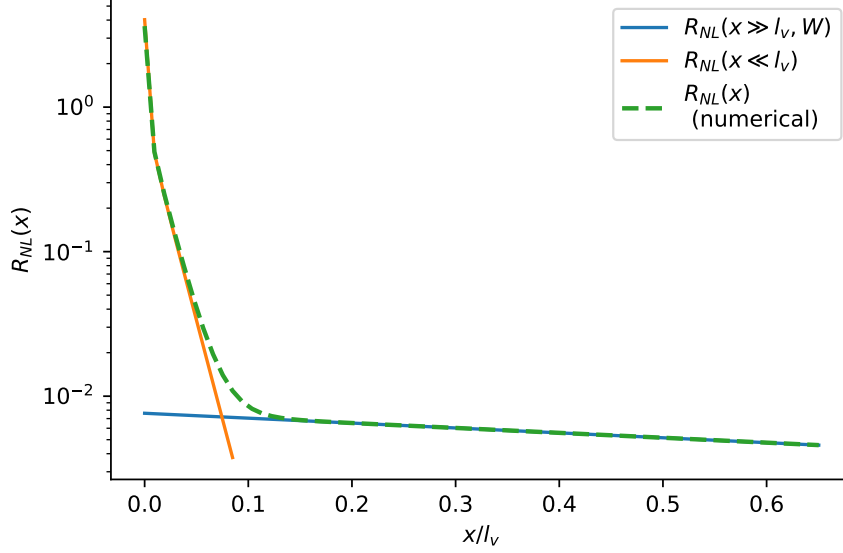
Figure 3.3: The parameters for this graph are exactly the same for the previous graph (figure 3.2)

choose are $k = 0$ and $k = +\infty$, since they are the points where the approximations work better. For doing the calculations it's best to write out the two approximations

$$R_{\mathrm{NL}}(k) \approx \alpha \frac{R_{xx}}{1 + L_{\mathrm{v}}^2 k^2} + \beta \frac{2\rho}{k} \tanh\left(\frac{kW}{2}\right) \cos^2(\theta_{\mathrm{VH}})$$

- For $k \to +\infty$ the term that is multiplied by β is an increasingly precise estimate of $R_{\mathrm{NL}}(k)$, and it dominates over the term that is multiplied by alpha, so $\beta = 1$.

- For $k = 0$ we have that

$$R_{xx} = \alpha R_{xx} + R_{xx} \cos^2(\theta_{\mathrm{VH}})$$

So, $\alpha = \sin^2(\theta_{\mathrm{VH}})$.

Putting it all together we define the resulting approximation

$$\boxed{\tilde{R}_{\mathrm{NL}}(k) \equiv \sin^2(\theta_{\mathrm{VH}}) R_{\mathrm{NL}}^T(k) + \cos^2(\theta_{\mathrm{VH}}) R_{\mathrm{NL}}^{(0)}(k)} \qquad (3.17)$$

The thing that I personally like about this approximation is its geometrical elegance. If we write all the terms of the equation above we get

$$\tilde{R}_{\mathrm{NL}}(k) \equiv \sin^2(\theta_{\mathrm{VH}}) \frac{R_{xx}}{1 + L_{\mathrm{v}}^2 k^2} + \cos^2(\theta_{\mathrm{VH}}) \frac{2\rho}{k} \tanh\left(\frac{kW}{2}\right) \qquad (3.18)$$

47

And if we plot the approximation $\tilde{R}_{\mathrm{NL}}(k)$ alongside the actual values of $R_{\mathrm{NL}}(k)$ we can see that they are remarkably similar (figure 3.4)
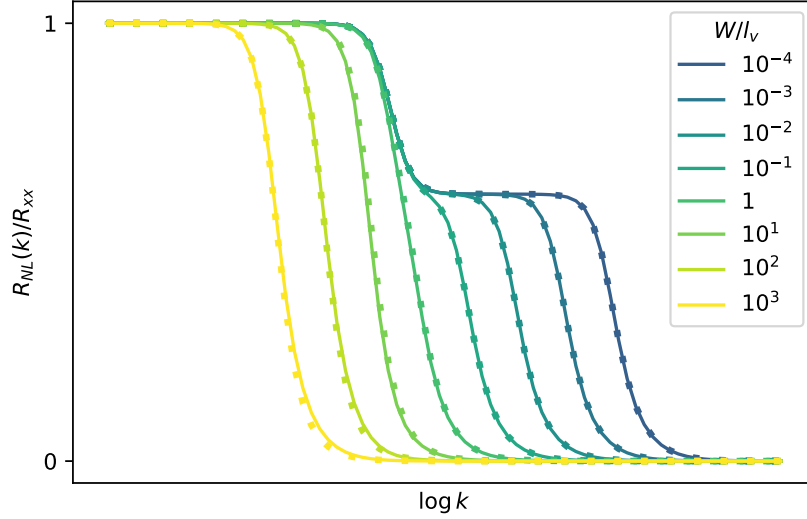

Figure 3.4: Comparison between $R_{\mathrm{NL}}(k)$ and $\tilde{R}_{\mathrm{NL}}(k)$. The continuous line represents $R_{\mathrm{NL}}(k)$, while the dashed line represents $\tilde{R}_{\mathrm{NL}}(k)$. It's unreasonably accurate!

The nice thing about this is that if two equations are similar, then their Fourier transform will be too. This means that $\tilde{R}_{\mathrm{NL}}(x)$ will be a good approximation of $R_{\mathrm{NL}}(x)$, where

$$\boxed{\tilde{R}_{\mathrm{NL}}(x) = \sin^2(\theta_{\mathrm{VH}}) R_{\mathrm{NL}}^T(x) + \cos^2(\theta_{\mathrm{VH}}) R_{\mathrm{NL}}^{(0)}(x)} \tag{3.19}$$

We can write out the full formula using equations 3.13 and 3.16

$$\tilde{R}_{\mathrm{NL}}(x) = \frac{R_{xx}}{2L_{\mathrm{v}}} e^{-|x|/L_{\mathrm{v}}} \sin^2(\theta_{\mathrm{VH}}) - \frac{2R_{xx}}{\pi W} \ln \left| \tanh \left(\frac{\pi x}{2W} \right) \right| \cos^2(\theta_{\mathrm{VH}}) \tag{3.20}$$

Infact if we re-create figure 3.3 with the equation above we get figure 3.5

3.2 $R_{\mathbf{NL}}(x)$ as we change ρ

Hall effect experiments are generally done in Hall-bars. These are samples of material with a shape like the one in figure 3.6, it also means that more often than not in experimental setups we cannot change x without changing the geometry of the sample.
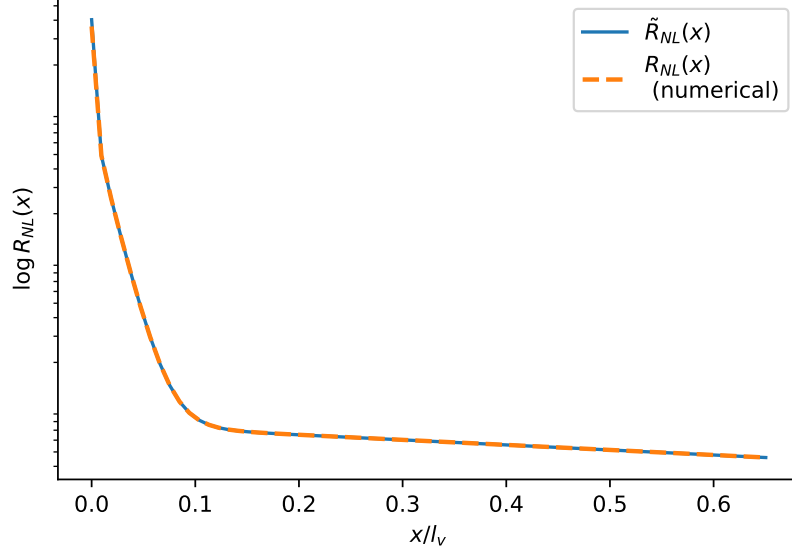
48

Figure 3.5: As you can see it's impossible to distinguish the difference between the two functions to the naked eye. The parameters are the same as figure 3.5
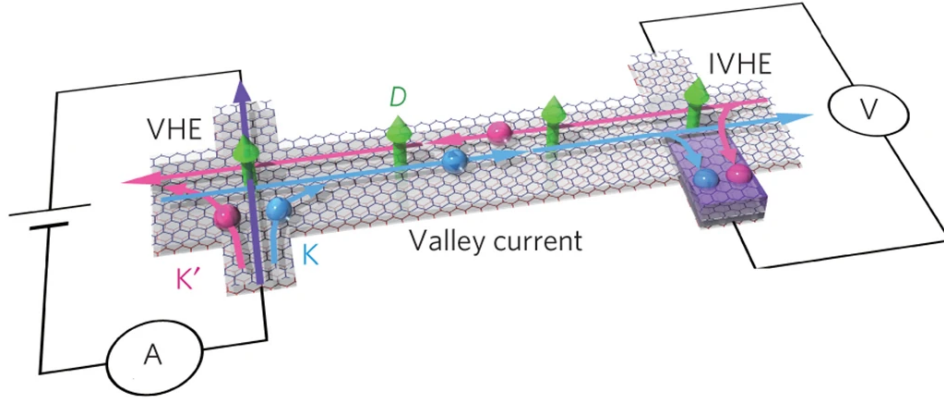

Figure 3.6: Example of Hall bar the currents are injected and measured in the rectangular contacts that come out from the main strip

In the previous section we studied how R_{NL} depended on x, but since Hall-bars can only measure a single x one of the ways to have multiple measurements with the same Hall-bar is to change the resistivity of the material by changing the temperature of the setup, and study R_{NL} as we change ρ_{xx}.

If you were to conduct an experiment where you measure R_{NL} as you change the resistivity of the material ρ you would have in general something that looks like figure 3.7.
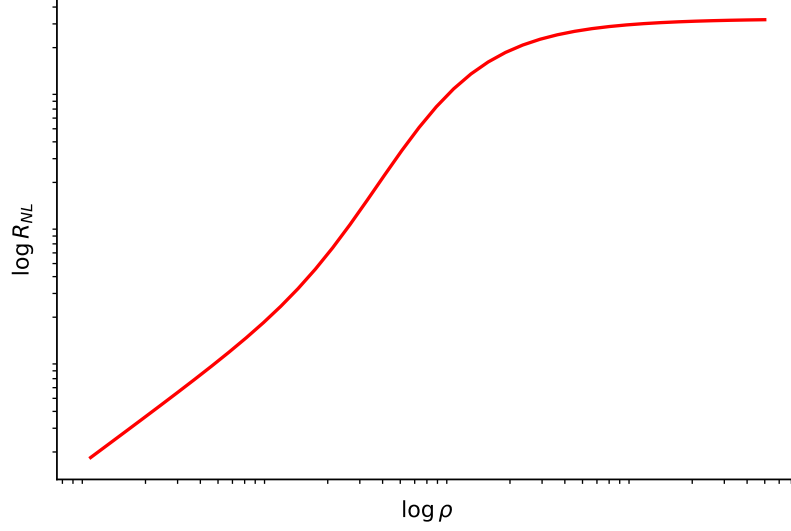
Figure 3.7: Looking at the image you can see that at the start it increases linearly, then it starts to increase even faster just before reaching a plateau.

The objective of this section is effectively to be able to understand this graph.

Just like before to understand the general behavior of $R_{\mathrm{NL}}(\rho)$ we'll examine $\rho \to 0$ and $\rho \to \infty$. For convenience let's re-write equation 3.1

$$R_{\mathrm{NL}}(k) = \frac{2\omega(k)}{k\sigma_c} \left\{ \frac{\omega(k)}{\tanh(kW/2)} + \frac{k\tan^2(\theta_{\mathrm{VH}})}{\tanh[\omega(k)W/2]} \right\}^{-1}$$

3.2.1 Low resistivity limit $(\rho \to 0)$

Sending $\rho \to 0$ is effectively equal to sending $\tan(\theta_{\mathrm{VH}}) = \sigma_{\mathrm{v}}\rho \to 0$. To be more precise we are going to assume that

$$\frac{k\tan^2(\theta_{\mathrm{VH}})}{\tanh[\omega(k)W/2]} \ll \frac{\omega(k)}{\tanh(kW/2)} \qquad \forall k$$

Which means that $\tan^2(\theta_{\mathrm{VH}}) \ll 1$. So now we do a Taylor series expansion of the above equation around $\tan^2(\theta_{\mathrm{VH}}) = 0$.

$$R_{\mathrm{NL}}(k) \approx R_{\mathrm{NL}}(k)|_{\tan^2(\theta_{\mathrm{VH}})=0} + \frac{\partial}{\partial\tan^2(\theta_{\mathrm{VH}})} R_{\mathrm{NL}}(k)|_{\tan^2(\theta_{\mathrm{VH}})=0}$$

that we are going to re-define as

$$R_{\mathrm{NL}}(k) \approx R_{\mathrm{NL}}^{(0)}(k) + R_{\mathrm{NL}}^{(1)}(k)\tan^2(\theta_{\mathrm{VH}})$$

The zeroth order term gives us our good old ohmic response in the frequency domain (eq. 3.2)

$$R_{\text{NL}}^{(0)}(k) = \frac{2\rho}{k} \tanh\left(\frac{kW}{2}\right)$$

This makes sense because as we lower ρ/ρ_{v} the hall current will be increasingly smaller and so the ohmic response will dominate.

And if we do the Fourier transform to get the x dependent form we get the ohmic nonlocal resistivity 2.22

$$R_{\text{NL}}^{(0)}(x) = \frac{2\rho}{\pi} \ln\left|\coth\left(\frac{\pi x}{2W}\right)\right| \tag{3.21}$$

Now let's calculate the first order term

$$R_{\text{NL}}^{(1)}(k)\tan^2(\theta_{\text{VH}}) = -2\rho\frac{\omega(k)}{k}\left[\frac{\omega(k)}{\tanh(Wk/2)}\right]^{-2} k\frac{\tan^2(\theta_{\text{VH}})}{\tanh(\omega(k)W/2)} =$$

$$= -2\rho^3\sigma_{\text{v}}^2\tanh^2\left(\frac{kW}{2}\right)\left\{\omega(k)\tanh\left[\frac{\omega(k)W}{2}\right]\right\}^{-1} \equiv \rho^3 F(k)$$

where $F(k)$ is defined as follows

$$F(k) \equiv -2\sigma_{\text{v}}^2\tanh^2\left(\frac{kW}{2}\right)\left\{\omega(k)\tanh\left[\frac{\omega(k)W}{2}\right]\right\}^{-1} \tag{3.22}$$

And it doesn't depend on ρ. Its Fourier transform is

$$F(x) = -2\sigma_v^2\int_{-\infty}^{+\infty}\tanh^2\left(\frac{kW}{2}\right)\left\{\tanh\left[\frac{\omega(k)W}{2}\right]\right\}^{-1}\frac{e^{-ikx}}{\omega(k)}\frac{dk}{2\pi} \tag{3.23}$$

Putting it all together we get that

$$\lim_{\rho\to 0} R_{\text{NL}}(x) = \frac{2\rho}{\pi}\ln\left|\coth\left(\frac{\pi x}{2W}\right)\right| + \rho^3 F(x) + o(\rho^5) \tag{3.24}$$

3.2.2 Large resistivity limit ($\rho \to \infty$)

Now let's study what happens when $\rho, \tan(\theta_{\text{VH}}) \to \infty$. First off let's rewrite equation 3.1 and bring the $\omega(k)$ and k inside the curly braces.

$$R_{\text{NL}}(k) = 2\rho\left\{\underbrace{\frac{k}{\tanh(kW/2)}}_{\substack{\text{cannot be} \\ \text{ignored for } k=0}} + \frac{k^2}{\omega(k)}\frac{\tan^2(\theta_{\text{VH}})}{\tanh[\omega(k)W/2]}\right\}^{-1} \tag{3.25}$$

This limit is a bit tricky to evaluate. First off even thought the rightmost term inside the curly braces dominates everywhere except for $k = 0$
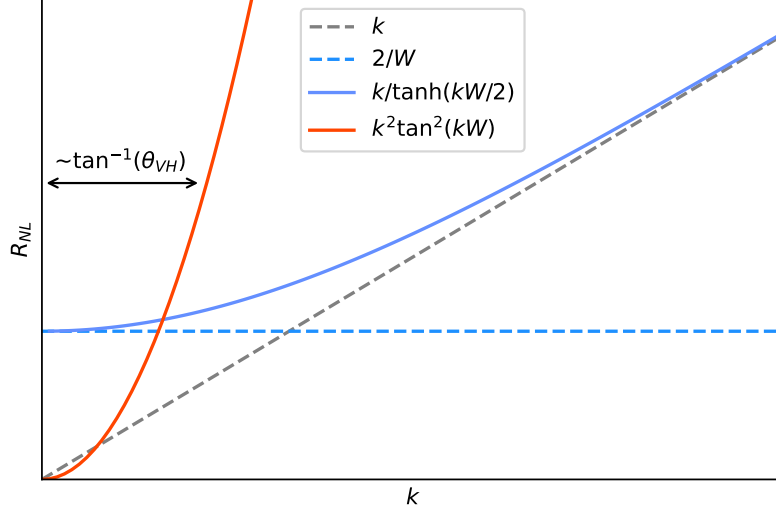
51

Figure 3.8: This graph shows the elements inside the curly brakets in equation 3.25. The continuous blue line represents the first term, the blue dashed line represents its approximation around $k = 0$ and the gray dashed lines represent its approximation for $k \to \infty$.

The orange parabola represents the right-hand side term $\frac{k^2}{\omega(k)} \frac{\tan^2(\theta_{\mathrm{VH}})}{\tanh[\omega(k)W/2]}$

this "*small detail*" is crucial. From image 3.8 we can see that the larger ρ gets, the smaller the area around $k = 0$ where the first term dominates.

For high values of $\rho, \tan(\theta_{\mathrm{VH}})$ the parabola becomes really narrow, and it overtakes the first term. This means that for the values of $\tan(\theta_{\mathrm{VH}})$ such that the parabola manages to overtake the $k \tanh^2(kW/2)$ term before $k = 2/W$ we can approximate the first term as being always equal to $2/W$. To be more precise

$$\left(\frac{2}{W}\right)^2 \frac{1}{\omega(2/W)} \frac{\tan^2(\theta_{\mathrm{VH}})}{\tanh[\omega(2/W)W/2]} \gg \frac{2}{W}$$

so,

$$\tan^2(\theta_{\mathrm{VH}}) \gg \sqrt{1 + \frac{W^2}{4l_{\mathrm{v}}^2}} \tanh\left(\sqrt{1 + \frac{W^2}{4l_{\mathrm{v}}^2}}\right) \tag{3.26}$$

This means that in that case

$$R_{\mathrm{NL}}(k) \approx 2\rho \left\{ \frac{2}{W} + \frac{k^2}{\omega(k)} \frac{\tan^2(\theta_{\mathrm{VH}})}{\tanh[\omega(k)W/2]} \right\}^{-1} \tag{3.27}$$

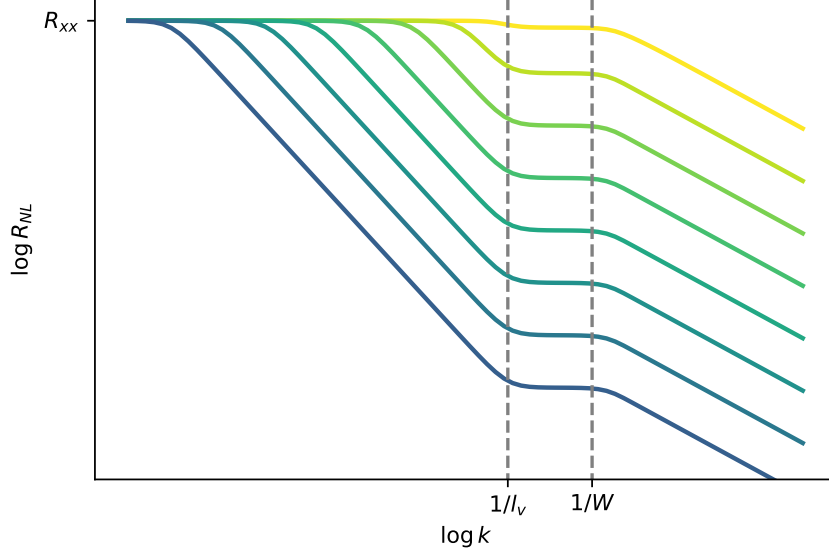Ok, low let's take a look at this function as we make ρ bigger and bigger

Figure 3.9: In this graph the darker the line color is, the bigger is the value of ρ. Notice how, as we increase ρ the first regime becomes more dominant

As you can see from figure 3.9 are three regimes here. The first one in for $k < l_{\mathrm{v}}^{-1}$, the second one is for $l_{\mathrm{v}}^{-1} < k < W^{-1}$ and the third one is for $W^{-1} < k$

First regime

In the first regime $(k < l_{\mathrm{v}}^{-1})$ $R_{\mathrm{NL}}(k)$ is similar to a Lorentzian function.

$$\lim_{\rho \to \infty} R_{\mathrm{NL}}(k) = 2\rho \left\{ \frac{2}{W} + l_{\mathrm{v}} k^2 \frac{\tan^2(\theta_{\mathrm{VH}})}{\tanh[W/2l_{\mathrm{v}}]} \right\}^{-1} \tag{3.28}$$

We can re-parametrize it As

$$\lim_{\rho \to \infty} R_{\mathrm{NL}}(k) = \frac{R_{xx}}{1 + (k/\Gamma)^2} \tag{3.29}$$

Where

$$\Gamma = \frac{1}{\tan(\theta_{\mathrm{VH}})} \sqrt{\frac{2}{l_{\mathrm{v}} W} \tanh\left(\frac{W}{2l_{\mathrm{v}}}\right)}$$

Therefore ρ and the standard deviation of the Lorentzian Γ are inversely proportional.

If we do the anti-Fourier transform of this equation to get the position dependent Non-local resistivity we get

$$\mathcal{F}^{-1}\left[\frac{R_{xx}}{1+(k/\Gamma)^2}\right] = \frac{1}{2}\rho W \Gamma e^{-|x|\Gamma} =$$

$$= \frac{\rho W}{\tan(\theta_{\mathrm{VH}})}\sqrt{\frac{2}{l_{\mathrm{v}}W}\tanh\left(\frac{W}{2l_{\mathrm{v}}}\right)}\exp\left[\frac{-|x|}{\tan(\theta_{\mathrm{VH}})}\sqrt{\frac{2}{l_{\mathrm{v}}W}\tanh\left(\frac{W}{2l_{\mathrm{v}}}\right)}\right] \quad (3.30)$$

Since $\tan(\theta_{\mathrm{VH}}) = \rho\sigma_{\mathrm{v}}$, for $\rho \to +\infty$ the equation above converges pointwise to the following saturation constant S

$$\lim_{\rho\to\infty}\mathcal{F}^{-1}\left[\frac{R_{xx}}{1+(k/\Gamma)^2}\right] = \frac{1}{\sigma_{\mathrm{v}}}\sqrt{\frac{2W}{l_{\mathrm{v}}}\tanh\left(\frac{W}{2l_{\mathrm{v}}}\right)} \equiv S \quad (3.31)$$

Second regime and third regime

Now that we have calculated how it behaves in the regime where is similar to a Lorenztian, let's calculate the second regime. We have already calculated the value the plateau assumes in equation 3.4

$$R_{\mathrm{NL}}(k) \approx \rho W \cos^2(\theta_{\mathrm{VH}}) \quad (3.32)$$

While in the third and last regime

$$R_{\mathrm{NL}}(k) \approx \frac{2\rho}{k}\cos^2(\theta_{\mathrm{VH}}) \quad (3.33)$$

Notice how the equations for the second and third regime are both proportional to $\rho\cos^2(\theta_{\mathrm{VH}})$. This means we can write equation 3.27 as approximately

$$\lim_{\rho\to\infty}R_{\mathrm{NL}}(k) = \frac{R_{xx}}{1+(k/\sigma)^2} + \rho\cos^2(\theta_{\mathrm{VH}})C(k) \quad (3.34)$$

Where $C(k)$ is a function that doesn't depend on ρ or $\tan(\theta_{\mathrm{VH}})$ and it comprehends the second, third regime and eventual corrections in between the approximations[1].

Now let $G(x)$ be it's Fourier anti-transform, then we have that

$$\lim_{\rho\to\infty}R_{\mathrm{NL}}(x) = S + \frac{1}{\rho}G(x) \quad (3.35)$$

Where here we have used that $\lim_{\rho\to\infty}\rho\cos^2(\theta_{\mathrm{VH}}) = 1/\rho$. This means that for $\rho \to +\infty$ the right hand side term vanishes, unless it diverges. And indeed $G(x)$ diverges for $x = 0$. Therefore, the limit above has pointwise convergence in $\{x \in \mathbb{R} \,|\, x \neq 0\}$

$$\lim_{\rho\to\infty}R_{\mathrm{NL}}(x) = \frac{1}{\sigma_{\mathrm{v}}}\sqrt{\frac{2W}{l_{\mathrm{v}}}\tanh\left(\frac{W}{2l_{\mathrm{v}}}\right)} \qquad \text{for } x \neq 0 \quad (3.36)$$

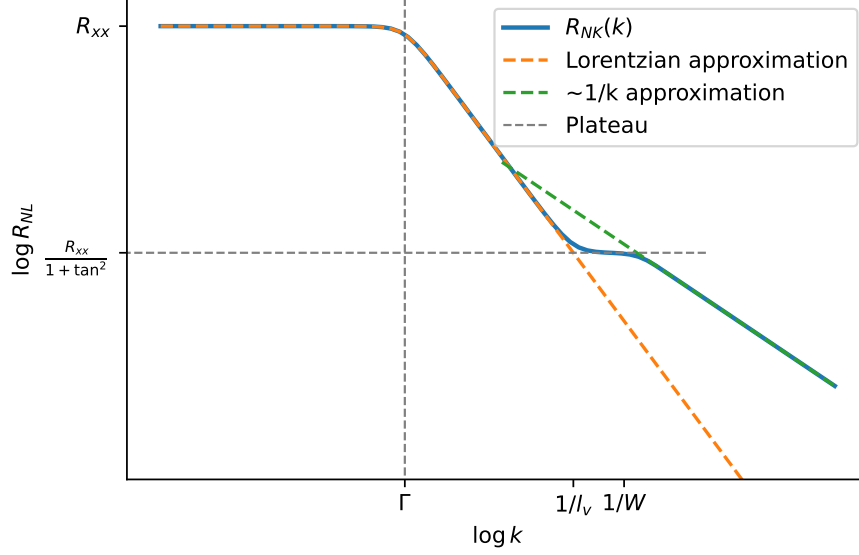[1]The corrections also are proportional to $\rho\cos^2(\theta_{\mathrm{VH}})$

Figure 3.10: The main regimes of this function

3.2.3 Putting it all together

The main result from subsection 3.2.1 we showed that for $\tan^2(\theta_{\mathrm{VH}}) \ll 1$ we had equation 3.24

$$R_{\mathrm{NL}}(x) = \frac{2\rho}{\pi} \ln \left| \coth \left(\frac{\pi x}{2W} \right) \right| + \rho^3 F(x) + o(\rho^5)$$

While, in subsection 3.2.2 we had that for $\tan^2(\theta_{\mathrm{VH}}) \gg \sqrt{1 + W^2/(4l_{\mathrm{v}}^2)} \tanh \left(\sqrt{1 + W^2/(4l_{\mathrm{v}}^2)} \right)$ (eq. 3.26) we had equation 3.36.

$$R_{\mathrm{NL}}(x) = \frac{1}{\sigma_{\mathrm{v}}} \sqrt{\frac{2W}{l_{\mathrm{v}}} \tanh \left(\frac{W}{2l_{\mathrm{v}}} \right)}$$

If we plot the approximations on top of the actual function we get something that looks like figure 3.11

3.2.4 Altertative way of studying $R_{\mathbf{NL}}(x)$ as we change ρ

Up until now we have studied $R_{\mathrm{NL}}(x)$ as we change ρ starting directly from the frequency response function (eq. 3.1). This is the most rigorous way for doing this analysis, but it can be cumbersome to work with and doesn't really offer much insight in the topology behind.
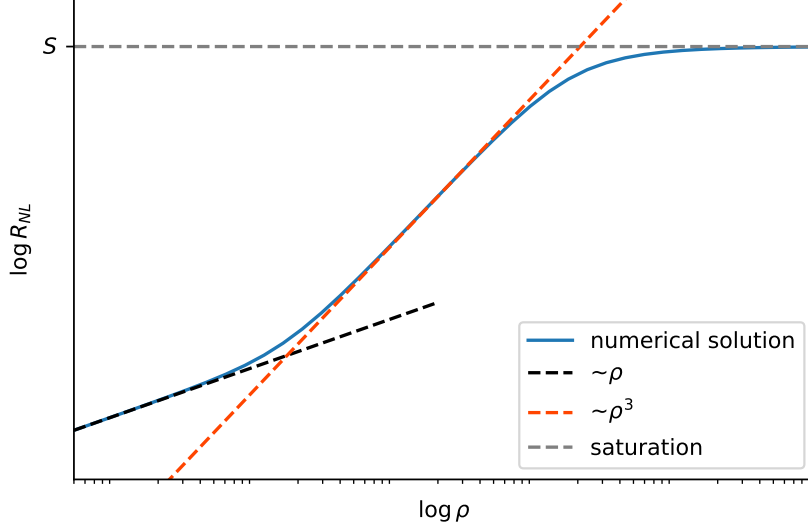
Figure 3.11: The main regimes of this function

A much simpler, but less rigorous way of approaching the problem would be to start from the approximate form of $R_{\mathrm{NL}}(x)$ (eq. 3.19). As you might remeber, this equation had the advantage of being able to distinguish the ohmic effect from the topological ones giving us a strong tool to be able to analyze the graphs.

From image 3.12 it is clear that the linear part at low $\tan(\theta_{\mathrm{VH}})$ is due to the ohmic effect. This makes sense even intuitively, infact the current will prefer choosing the path of least resistance, and since at low $\tan(\theta_{\mathrm{VH}})$ the ohmic resistivity is much less than the hall resistivity, we have a mostly ohmic behavior.

This image also shows that the topological component is the one responsible for the ρ^3 behavior, and then the saturation value.

A few small details

In the discussion about R_{NL} as we change ρ we choose parameters to highlight the behaviors we talked about. However sometimes certain behaviors disappear, for example if we increase the ohmic contributions by decreasing the width of the bar, figures 3.11 and 3.12 become like in figure 3.13

In the following section we'll see how this applies to lab measurements
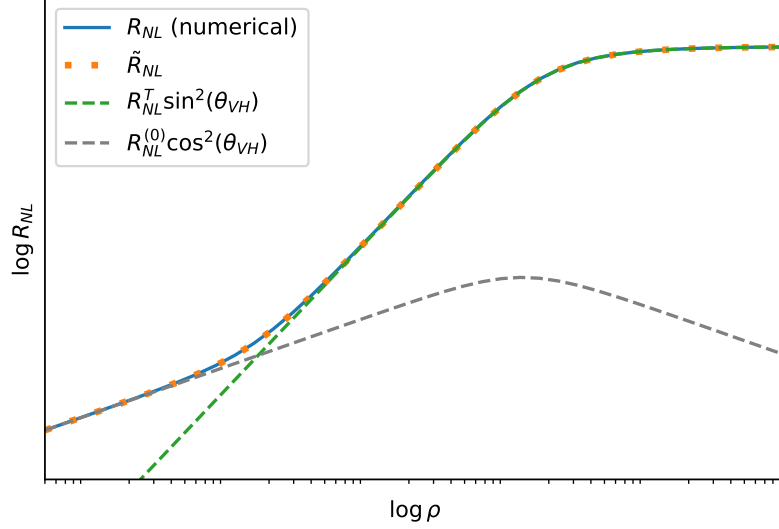
Figure 3.12: R_{NL} (continuous blue line, calculated numerically) and its approximation $\tilde{R}_{\mathrm{NL}}$ (dotted orange line) are virtually indistinguishable. The topological component of $\tilde{R}_{\mathrm{NL}}$ is the green dashed line and the ohmic is the grey dashed line.

3.2.5 Shortcomings of the model

The main shortcoming of the model is that we don't explore the temperature dependence of the system, while we can expect that such effect to be noticeble will need to happen at low temperature CONTINUA

Does this generalize?

Up until now we talked about valley currents, however this also applies to spin-hall effect and spin-orbit effect since the differential equations that govern the system are equivalent

3.3 Comparison with experimental data

Experimental setups have a few limitations compared to the theoretical treatment, for example you don't have complete freedom of changing the resistance, rather the resistance is changed by changing the temperature of the sample. This has a few consequences:

- Since out sample is a semiconductor, the lower the temperature, the higher the resistance, but if the temperature gets too low we enter the ballistic regime, and our treatment is no longer valid.
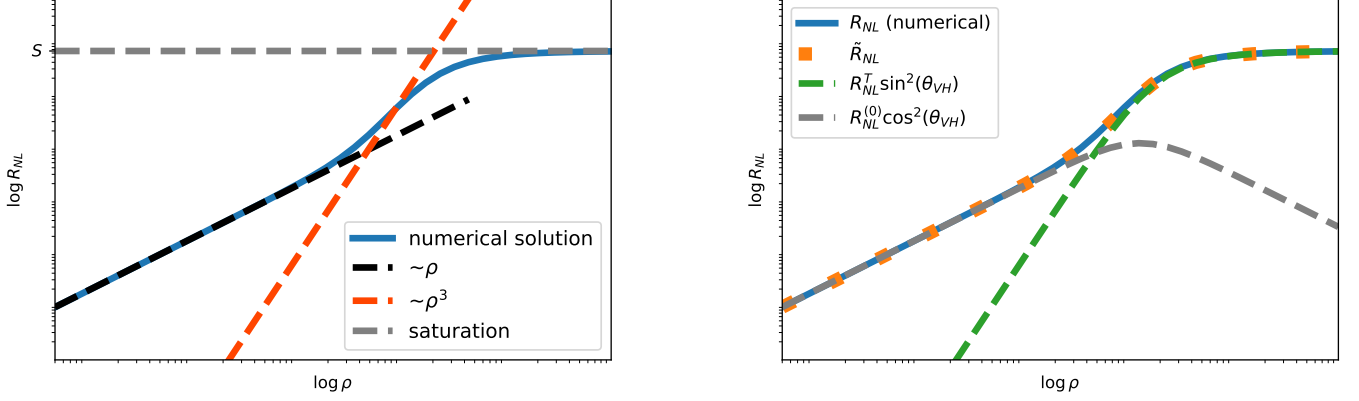
Figure 3.13: As you can see the ρ^3 behavior disappeared

- If the temperature gets too high, the quantization of the hall effect disappears

This restricts us to a couple order of magnitude of the resistivity.

Now we compare the results with the experimental data. Let's start from analyzing the data from [36].

In this paper the authors measured the valley hall effect of a heterostructure made of bilayer-graphene on top of boron nitride at different angles ϕ between the graphene and the boron nitride. The sample has a width $W = 1.7\mu$m, and inter-valley scattering length $l_{\mathrm{v}} = 1.6\mu$m and the distance of the contact from the injection point is $x = 2.3\mu$m

The angles ϕ that were explored are $0, \pi/6$ and $\pi/3$. If you plot the measurements you get figure 3.14

Now we analyze them one by one

- For $\phi = \pi/3$ we have that the response is fully ohmic, and so we get a completely linear response (figure 3.15)

- For $\phi = \pi/6$ we have a hall effect, however, since $W \approx l_{\mathrm{v}}$ the ohmic and the topological response mix together, so we never see the full-fledged ρ^3 behavior.[2]

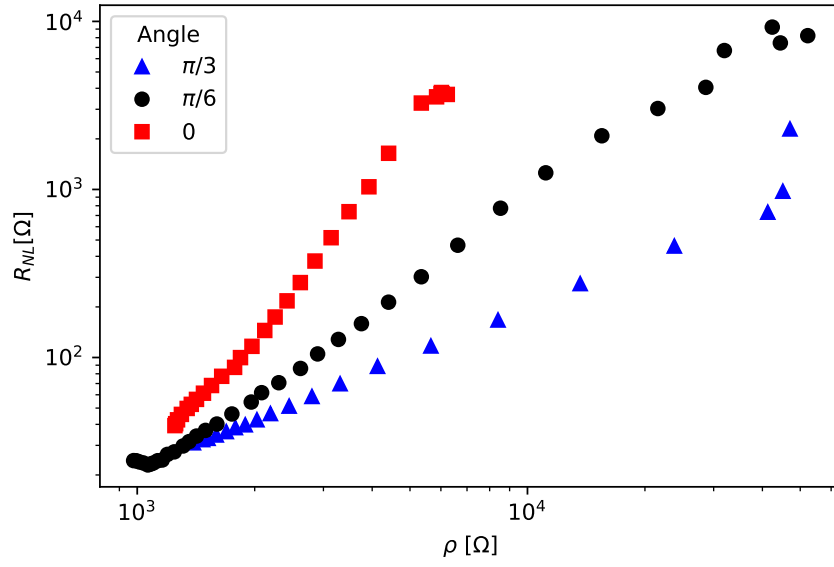[2]A more detailed explanation was given in the details of subsection 3.2.4

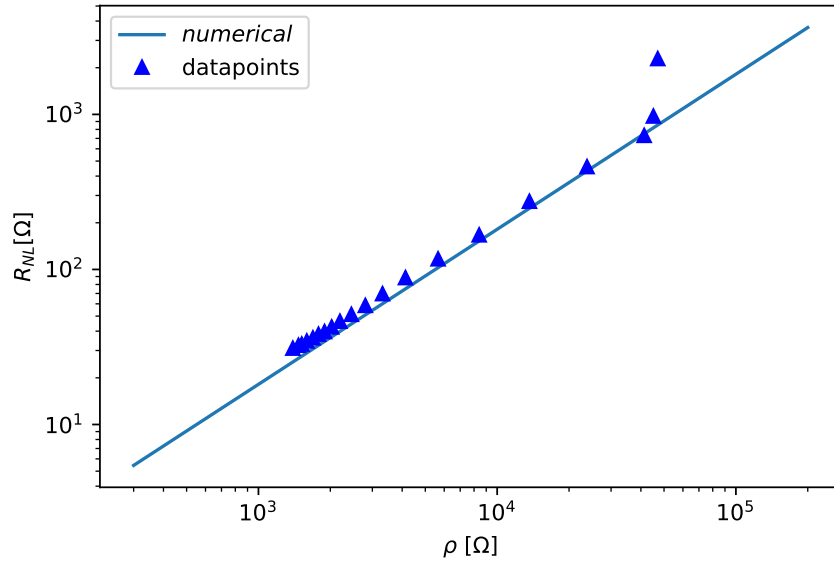**Figure 3.14:** Datapoints from [36]

Figure 3.15: Comparison between the data points and the theoretical expectation for $\phi = \pi/3$. The last point is an outlier, but all in all it looks pretty good
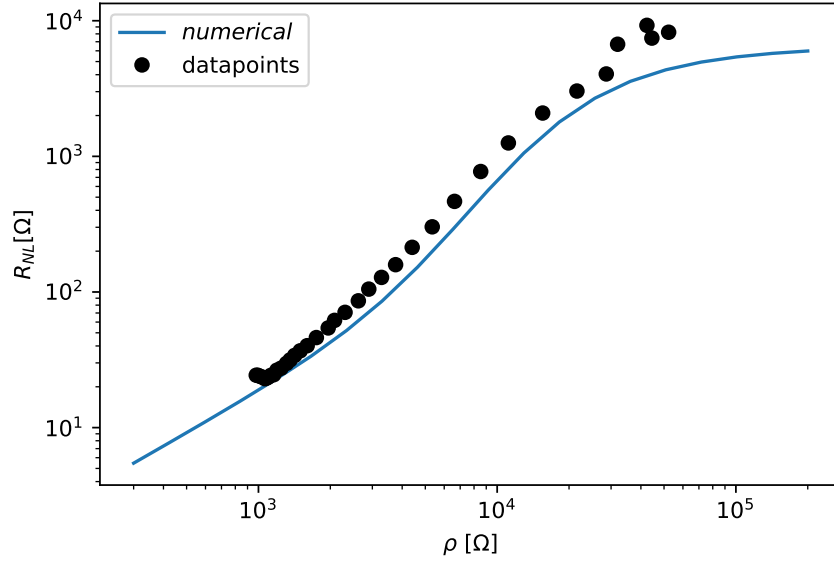
Figure 3.16: Comparison between the data points and the theoretical expectation for $\phi = \pi/6$. The model has a lower precision for higher values of ρ, R_{NL}

Bibliography

[1] D. Tong, "Lectures on the quantum hall effect," *arXiv preprint arXiv:1606.06687*, 2016.

[2] S. Weinberg, *Lectures on Quantum Mechanics*. Hyperion New York, 2013.

[3] D. J. Thouless, M. Kohmoto, M. P. Nightingale, and M. den Nijs, "Quantized hall conductance in a two-dimensional periodic potential," *Physical review letters*, vol. 49, no. 6, p. 405, 1982.

[4] K. S. Novoselov *et al.*, "Electric field effect in atomically thin carbon films," *Science*, vol. 306, no. 5696, pp. 666–669, 2004. DOI: `10.1126/science.1102896`. eprint: `https://www.science.org/doi/pdf/10.1126/science.1102896`. [Online]. Available: `https://www.science.org/doi/abs/10.1126/science.1102896`.

[5] A. H. Castro Neto, F. Guinea, N. M. R. Peres, K. S. Novoselov, and A. K. Geim, "The electronic properties of graphene," *Rev. Mod. Phys.*, vol. 81, pp. 109–162, 1 2009. DOI: `10.1103/RevModPhys.81.109`. [Online]. Available: `https://link.aps.org/doi/10.1103/RevModPhys.81.109`.

[6] F. Bloch, "Über die quantenmechanik der elektronen in kristallgittern," *Zeitschrift für physik*, vol. 52, no. 7, pp. 555–600, 1929.

[7] J. C. Slater and G. F. Koster, "Simplified lcao method for the periodic potential problem," *Physical Review*, vol. 94, no. 6, p. 1498, 1954.

[8] G. Grosso and G. P. Parravicini, *Solid state physics*. Academic press, 2013.

[9] E. McCann and M. Koshino, "The electronic properties of bilayer graphene," *Reports on Progress in Physics*, vol. 76, no. 5, p. 056 503, 2013. DOI: `10.1088/0034-4885/76/5/056503`. [Online]. Available: `https://doi.org/10.1088%2F0034-4885%2F76%2F5%2F056503`.

[10] A. Kuzmenko, I. Crassee, D. Van Der Marel, P Blake, and K. Novoselov, "Determination of the gate-tunable band gap and tight-binding parameters in bilayer graphene using infrared spectroscopy," *Physical Review B*, vol. 80, no. 16, p. 165 406, 2009.

[11] D. Vanderbilt, *Berry phases in electronic structure theory: electric polarization, orbital magnetization and topological insulators*. Cambridge University Press, 2018.

[12] E. H. Hall, "Xviii. on the "rotational coefficient" in nickel and cobalt," *The London, Edinburgh, and Dublin Philosophical Magazine and Journal of Science*, vol. 12, no. 74, pp. 157–172, 1881.

[13] R. Karplus and J. Luttinger, "Hall effect in ferromagnetics," *Physical Review*, vol. 95, no. 5, p. 1154, 1954.

[14] P. B. Smith, "The resonant scattering integral; application to the analysis of elastic proton scattering," *Physica*, vol. 24, no. 6-10, pp. 1085–1091, 1958.

[15] L. Berger, "Side-jump mechanism for the hall effect of ferromagnets," *Physical Review B*, vol. 2, no. 11, p. 4559, 1970.

[16] N. Nagaosa, J. Sinova, S. Onoda, A. H. MacDonald, and N. P. Ong, "Anomalous hall effect," *Reviews of modern physics*, vol. 82, no. 2, p. 1539, 2010.

[17] V. Dugaev, P Bruno, M Taillefumier, B Canals, and C Lacroix, "Anomalous hall effect in a two-dimensional electron gas with spin-orbit interaction," *Physical Review B*, vol. 71, no. 22, p. 224 423, 2005.

[18] Y. Tian, L. Ye, and X. Jin, "Proper scaling of the anomalous hall effect," *Physical review letters*, vol. 103, no. 8, p. 087 206, 2009.

[19] M. D'yakonov and V. Perel, "Spin orientation of electrons associated with the interband absorption of light in semiconductors," *Soviet Journal of Experimental and Theoretical Physics*, vol. 33, p. 1053, 1971.

[20] S. Wolf *et al.*, "Spintronics: A spin-based electronics vision for the future," *science*, vol. 294, no. 5546, pp. 1488–1495, 2001.

[21] Y. A. Bychkov and É. I. Rashba, "Properties of a 2d electron gas with lifted spectral degeneracy," *JETP lett*, vol. 39, no. 2, p. 78, 1984.

[22] C. L. Kane and E. J. Mele, "Quantum spin hall effect in graphene," *Physical review letters*, vol. 95, no. 22, p. 226 801, 2005.

[23] R. Gorbachev *et al.*, "Detecting topological currents in graphene superlattices," *Science*, vol. 346, no. 6208, pp. 448–451, 2014.

[24] M. Sui *et al.*, "Gate-tunable topological valley transport in bilayer graphene," *Nature Physics*, vol. 11, no. 12, pp. 1027–1031, 2015.

[25] Y. Shimazaki, M. Yamamoto, I. V. Borzenets, K. Watanabe, T. Taniguchi, and S. Tarucha, "Generation and detection of pure valley current by electrically induced berry curvature in bilayer graphene," *Nature Physics*, vol. 11, no. 12, pp. 1032–1036, 2015.

[26]   D. Xiao, G.-B. Liu, W. Feng, X. Xu, and W. Yao, "Coupled spin and valley physics in monolayers of mos 2 and other group-vi dichalcogenides," *Physical review letters*, vol. 108, no. 19, p. 196 802, 2012.

[27]   K. F. Mak, K. L. McGill, J. Park, and P. L. McEuen, "The valley hall effect in mos2 transistors," *Science*, vol. 344, no. 6191, pp. 1489–1492, 2014.

[28]   J. Lee, Z. Wang, H. Xie, K. F. Mak, and J. Shan, "Valley magnetoelectricity in single-layer mos2," *Nature materials*, vol. 16, no. 9, pp. 887–891, 2017.

[29]   S. O. Valenzuela and M Tinkham, "Direct electronic measurement of the spin hall effect," *Nature*, vol. 442, no. 7099, pp. 176–179, 2006.

[30]   D. Abanin, A. Shytov, L. Levitov, and B. Halperin, "Nonlocal charge transport mediated by spin diffusion in the spin hall effect regime," *Physical review B*, vol. 79, no. 3, p. 035 304, 2009.

[31]   C Brüne *et al.*, "Evidence for the ballistic intrinsic spin hall effect in hgte nanostructures," *Nature Physics*, vol. 6, no. 6, pp. 448–454, 2010.

[32]   D. Abanin *et al.*, "Giant nonlocality near the dirac point in graphene," *Science*, vol. 332, no. 6027, pp. 328–330, 2011.

[33]   J. Balakrishnan and K. W. Koon, "G., jaiswal, m., castro neto, ah & özyilmaz, b. colossal enhancement of spin–orbit coupling in weakly hydrogenated graphene," *Nat. Phys*, vol. 9, pp. 284–287, 2013.

[34]   Z. Wang, C. Tang, R. Sachs, Y. Barlas, and J. Shi, "Proximity-induced ferromagnetism in graphene revealed by the anomalous hall effect," *Physical review letters*, vol. 114, no. 1, p. 016 603, 2015.

[35]   M. Beconcini, F. Taddei, and M. Polini, "Nonlocal topological valley transport at large valley hall angles," *Physical Review B*, vol. 94, no. 12, 2016. DOI: `10.1103/physrevb.94.121408`. [Online]. Available: `https://doi.org/10.1103%2Fphysrevb.94.121408`.

[36]   E. Arrighi *et al.*, "Non-identical moiré twins in bilayer graphene," 2022. DOI: `10.48550/ARXIV.2205.01760`. [Online]. Available: `https://arxiv.org/abs/2205.01760`.